ESCOLA NAVAL

talant de bien faire

Miguel Dias Ribeiro

Antenna Array for a Passive SAR System

A dissertation submitted in partial fulfillment of the requirements for the degree of Marine Military Sciences, specialisation of Engenharia Naval Ramo de Armas e Eletrónica

Alfeite

2022

Miguel Dias Ribeiro

Antenna Array for a Passive SAR System

A dissertation submitted in partial fulfillment of the requirements for the degree of Marine Military Sciences, specialisation of Engenharia Naval Ramo de Armas e Eletrónica

Orientation of: João Manuel de Almeida Monteiro Felício
Co-orientation of: Custódio José Oliveira Peixeiro

The Supervisor,

Assinado por : **João Manuel de Almeida Monteiro Felício**
Num. de Identificação: 13726816

João Felício

The Master Student,

Miguel Dias Ribeiro

The Co-Supervisor,

Custódio Peixeiro

Alfeite
2022

"Nothing in life is to be feared, it is only to be understood. Now is the time to understand more, so that we may fear less." — Marie Curie

First of all, I would like to thank my family and friends that gave me their full support throughout this journey. A special thanks to my mother that always pushed me up to accomplish my goals.

To my supervisor, Professor João Felício, for having accepted me in this challenge and for all his time dedicated to me.

To my co-supervisor, Professor Custódio Peixeiro, for having supported and helped me to overcome some of the difficulties throughout this project.

To the Instituto Superior Técnico and their personnel, for the access to their facilities and equipment in order to accomplish the objectives of this project.

To my three classmates and specially friends, Vitorino, Melo and Stattmiller, for all the good (and bad) moments that we spent together throughout these last five years.

Acknowledgement

I acknowledge the support of Instituto de Telecomunicacões (IT), under project UIDB/50008/2020, for access to all the required material and facilities, including laboratories, software and hardware equipment.

Abstract

In this thesis, the design of an array of antennas for a passive radar system is presented. The need to reinforce the ability of monitoring the maritime space with a low-cost, low-profile and light-weight passive synthetic aperture radar (SAR) motivated this work to be assembled on an Unmanned Aerial Vehicle (UAV), so that it can track ships and other vessels by the coastline, thus preventing illicit activities. This study focuses on the design and assessment of low-profile planar antenna arrays for passive radars at ISM-band of 2.45 GHz. The analytical formulation of the design of a stand-alone patch antenna is performed, which is followed by the detailed formulation of uniform and Chebyshev antenna arrays, including their feeding network and guidelines to obtain proper impedance matching. It is well-known that uniform arrays suffer from high sidelobe level, which may affect the detection of targets. As an alternative, we focus on the design of Chebyshev arrays, in order to achieve lower side lobe level, in the interest of increasing the probability of ambiguous detections and better tracking of the targets. Both arrays are designed and optimized through full-wave simulations using Computer Simulation Technology (CST). Good impedance matching at 2.45 GHz is obtained for both numerical and experimental results. Regarding the radiation pattern, the experimental assessment confirmed the right sidelobe level for the uniform array, although there are differences for the Chebyshev due to limitations in the measurement setup. Future work should include the optimization of the sidelobe level of the Chebyshev array.

Keywords: Passive Radar, Antenna Array, Patch Antenna, Chebyshev Design Method

Resumo

Nesta tese, é apresentado o projeto de um agregado de antenas para um sistema de radar passivo. A necessidade de reforçar a capacidade de monitorização do espaço marítimo com um radar de abertura sintética (SAR) passivo de baixo custo, baixo perfil e baixo peso motivou a implementação deste trabalho num Veículo Aéreo Não Tripulado (UAV), para que possa fazer o seguimento de navios e outras embarcações pela orla costeira, evitando assim atividades ilícitas. Este estudo concentra-se no projeto e avaliação de agregados de antenas planares de baixo perfil para radares passivos na banda ISM de 2.45 GHz. A formulação analítica do projeto de uma antena patch com um elemento isolado é realizada, seguida pela formulação detalhada de agregados de antenas uniformes e Chebyshev, incluindo as suas redes de alimentação e diretrizes para obter a adequada adaptação de impedâncias. É bem sabido que os agregados uniformes sofrem de um elevado nível de lobos secundários, o que pode afetar a detecção de alvos. Como alternativa, focamos no projeto em agregados de Chebyshev, a fim de atingir um nível de lobos secundários inferior, com o interesse de aumentar a probabilidade de detecções ambíguas e melhor seguimento dos alvos. Ambos os agregados são projetados e otimizados por meio de simulações de onda completa usando o *Computer Simulation Technology (CST)*. Uma boa adaptação de impedâncias em 2.45 GHz foi obtida para resultados numéricos e experimentais. Em relação ao diagrama de radiação, a avaliação experimental confirmou o nível certo de lobos secundários para o agregado uniforme, embora existam diferenças para o agregado de Chebyshev devido a limitações na configuração da medição. Trabalhos futuros devem incluir a otimização do nível de lobos secundários do agregado de Chebyshev.

Palavras-chave: Radar Passivo, Agregado de Antenas, Antena Patch, Método Chebyshev

Contents

List of Figures

List of Tables

List of Acronyms

BBC	**B**ritish **B**roadcasting **C**orporation
CST	**C**omputer **S**imulation **T**echnology
DAB	**D**igital **A**udio **B**roadcast
DVB-T	**D**igital **V**ideo **B**roadcast - **T**errestrial
FBR	**F**ront-to-**B**ack **R**atio
FM	**F**requency **M**odulated
PCR	**P**assive **C**overt **R**adar
RAF	**R**oyal **A**ir **F**orce
RCS	**R**adar **C**ross **S**ection
SAR	**S**inthetic **A**perture **R**adar
SLL	**S**ide **L**obe **L**evel
UAV	**U**nmanned **A**erial **V**ehicle
UHF	**U**ltra **H**igh **F**requency
VHF	**V**ery **H**igh **F**requency

Chapter 1

Introduction

1.1 Motivation and Objectives

This dissertation contains a study about passive radars and its usefulness to the Portuguese Navy. The characteristics that this type of radar offers allow the Navy to operate in a more silent and stealth environment in order to reinforce the ability of monitoring the maritime space with a low-cost passive synthetic aperture radar (SAR). This radar has to have the ability to be set on an Unmanned Aerial Vehicle (UAV) so that it can track ships and other vessels by the coastline, as illustrated in Fig. 1.1

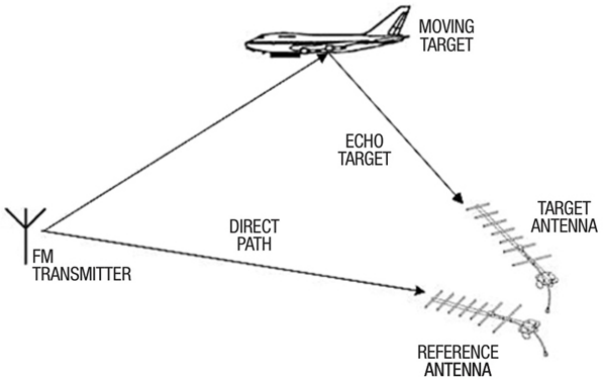

FIGURE 1.1: Bi-static passive radar scheme *in https://www.quora.com/What-is-passive-radar*

The main goal of this dissertation is to design an antenna array with a narrow beam and a low side lobe level that can be used in passive radar systems. As shown in Fig. 1.1, an electromagnetic wave is emitted by the FM transmitter which is, for example, a DVB-T station, and is received by the reference antenna. This wave will reflect on the target and the echo will be received by the target antenna. This target antenna is what this dissertation is focused on. A target antenna with a low side lobe level increases the probability of ambiguous detections

and a narrow beam allows a better tracking of the target as well as a better image. These characteristics can be archived by using the Chebyshev design method were it will be compared to a more standard design. Already existing radio frequencies, like DVB-T, will be used to develop this project. This kind of technology has a wide range of use in the civilian and military world.

To fulfil the objectives of the thesis, a deep study will be done in the areas of passive radars, design of a patch antennas (single element and arrays), antenna simulation and the corresponding experimental validation.

1.2 Framework

1.2.1 Passive Radars

Passive radars, unlike active radars, do not transmit any radiation to detect targets. Instead, they use existing transmitters mostly operating in the VHF or UHF bands and a network of receivers. This type of radar technology became attractive in the Second World War due to its way of detecting enemy airplanes without exposing ones location. Sir Robert Watson-Watt was the father of the innovating Daventry experiment, in which he used the electromagnetic wave from an already existing emitter (from the British Broadcasting Corporation, or BBC) to detect the Heyford bomber aircraft. After the successful experiment, the Royal Air Force (RAF) installed the well-known Chain Home radars in the coast of England to detect enemy aircraft during the World War II (Kuschel & O'Hagan, 2010; Kuschel et al., 2019).

With the invention of the duplexer in 1936, the interest in passive radar technology began to decrease. Later on, NATO brought it back in the 1990s with the discovery that the anti-stealthiness capability of this system could be an advantage in detecting stealth aircraft. Those aircraft had a reduced Radar Cross Section (RCS), which the bi- or multi-static passive radars were able to counter-stealth, unlike mono-static radars.

Those passive radars used an already existent broadcast transmitter, such as analogue television, as a VHF/UHF illuminator. Since then, Passive Covert Radar (PCR) system designs were tested to exploit its effectiveness using FM-radio signals. The FM broadcast stations could emit sufficient power to detect the targets, but the bandwidth emitted would change according to the type of transmission like voice, music or other (Kuschel & O'Hagan, 2010; Kuschel et al., 2019).

Commercial prototypes using FM-radio broadcast began to appear and were developed by French (C&T and Thales) and American (Lockheed-Martin) companies in the military field. After the exploit of the FM-radio signals, digital transmitters presented a constant bandwidth and some predictable characteristics like range, Doppler and sidelobe level (Kuschel & O'Hagan, 2010).

The first PCR system using digital broadcasting emitters (DVB-T and DAB) to detect air and maritime targets was the CORA system developed by FGAN-FHR (now Fraunhofer-FHR), a German company driven to explore the fields of high frequency physics and radar techniques. In 2006, the company made a measurement campaign where they realized that the system could offer resolutions of 100 m or 20 m using DAB or DVB-T, respectively. Those resolutions were much better than the resolutions offered by FM-radio broadcast. However, DAB stations emitted at a much lower power than DVB-T stations, making DVB-T emitters better for the job (Kuschel & O'Hagan, 2010).

Experimental results were obtained using DVB-T emitters for a passive SAR imaging technique (Kuschel & O'Hagan, 2010; Kuschel et al., 2019). The results showed that passive SAR systems have advantages when compared to active SAR systems due to its silent operation, as well as the usage of relatively low-frequency which helps to visualize concealed targets. The results also showed that there are some disadvantages when using passive radars: if the emitter is to close to the ground, some areas can be shadowed and the system requires a high computational power due to the complex signal processing (Gromek et al., 2016).

1.2.2 Chebyshev Method

Uniform arrays do not allow to control the side lobe level (SLL). It is well known that for N large the SLL of an uniform array tends to -13.5 dB. Such SLL value is not adequate for radar applications. The Chebyshev method is used to design arrays for a given side lobe level. This method is composed by five steps and uses the array factor to determine the cosine terms. These cosine terms are later used alongside with the Chebyshev polynomials to determine the excitation coefficients of the elements.

With this method, one can design nonuniform arrays still having a fixed spacing between elements like an uniform array, making possible to only vary the excitation between the elements (Tsoulos & Christodoulou, 2007).

1.3 Experimental Validation

After the design of both the uniform and the Chebyshev arrays, one of the goals of this dissertation is to fabricate a prototype for each of the two patch antennas and make the measurements needed to allow a comparison between the two arrays and verify if the Chebyshev design method can be used in further applications.

1.4 Dissertation Structure

This dissertation is divided in five chapters. This first chapter is an introduction to the topic of the thesis where the motivation and framework is presented, as well as the state of the art on passive radars and the Chebyshev method.

The second chapter contains the analytical formulation of the antenna problem. In this chapter, the formulation of a generalized antenna for passive radar systems will exploited together with the analytical formulation of a stand-alone patch antenna, a planar array design and the feeding network.

The third chapter deals with the numeric validation and optimization of the arrays. Similarly to the second chapter, a numeric simulation will be made to a stand-alone element, an uniform planar array and a Chebyshev planar array. The optimization will be made only to the last two, where in the next chapter these will be validated experimentally.

In chapter four, the prototypes will be fabricated and the measurements will take place. The comparison between the results obtained in chapter 3 (simulation) and this chapter (experimental) will also be presented.

Finally, the conclusions will come in chapter five where the results are talked about and a future work will be suggested.

Chapter 2

Analytical Formulation

One of the most common elements in printed circuits planar arrays are the microstrip patches. Microstrip antennas have a metallic patch printed on a dielectric substrate with a ground plane on the opposite side. This metallic patch can have various forms, depending on the user's final goal. Patch antennas are a commonly used type of antennas since they are cheap, easy to make and have a low profile (Orfanidis, 2004; Tsoulos & Christodoulou, 2007).

In this chapter, an analytical formulation is presented to design a patch antenna and all of its dimensions, an uniform array and a non-uniform array with the Chebyshev design method. All of the characteristics of their feeding network are also explored in this chapter.

2.1 Stand-Alone Patch Antenna

The initial step to design a stand-alone patch antenna is the isolated element. It is important to acknowledge that this patch antenna has only six parameters that dictate its shape as illustrated in Fig. 2.1. Note that the thickness of the ground plane can also influence the performance of the antenna. The other two parameters are used to shape the microstrip feeding line: L_{ms} and W_{ms}. The substrate has two characteristics, the dielectric constant (or relative electric permittivity) – ϵ_r – and its thickness: h.

The dimensions of the parameters W and L are proportional to the wavelength. As so, W is initially calculated by

$$W = \frac{\lambda_0}{2}\sqrt{\frac{2}{\epsilon_r + 1}} \tag{2.1}$$

where λ_0 is the free-space wavelength calculated as c/f_0 and ϵ_r is the dielectric constant of the substrate (Orfanidis, 2004).

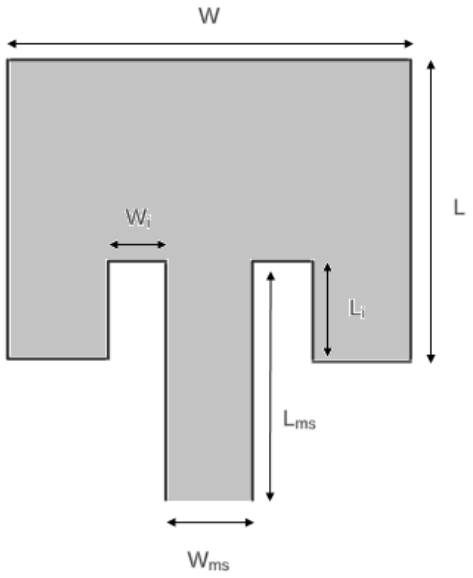

FIGURE 2.1: Patch antenna geometry

The electric field lines travel through the substrate from the patch to the ground plane, but they also travel through the air around, causing the *fringing* effect. To simplify the sizing of the antenna, one will consider an homogeneous and infinite environment where the effective permittivity – ϵ_{eff} – surrounds the printed circuit. Both cases are presented in Fig. 2.2.

The effective permittivity value is between 1 and ϵ_r, since the dielectric constant of the air is unitary. Looking at the two cases of Fig. 2.2, one concludes that if the substrate height is high, ϵ_{eff} gets closer to ϵ_r. On the other hand, if the substrate height is low, ϵ_{eff} tends to unity (Orfanidis, 2004).

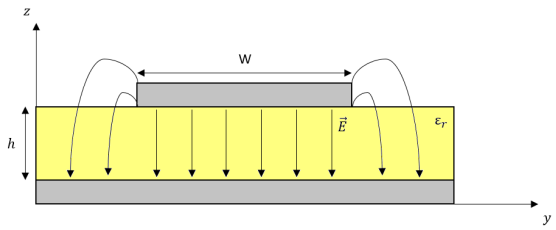

(A) actual transmission line printed on substrate of permittivity ϵ_r

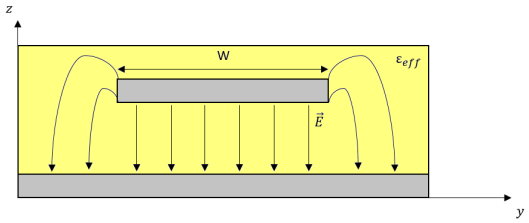

(B) effective permittivity model with effective permittivity ϵ_{eff}

FIGURE 2.2: Transmission line models

Equation 2.2 is used to calculate the effective permittivity. Note that these conclusions are valid only to thin substrates where $\frac{W}{h} > 1$ (Islam et al., 2018).

$$\epsilon_{eff} = \frac{\epsilon_r + 1}{2} + \frac{\epsilon_r - 1}{2}\left(1 + 12\frac{h}{W}\right)^{-1/2} \tag{2.2}$$

The next step is to get the value of the guided wavelength, λ_g. Due to the approximation represented in Fig. 2.2, the wavelength is affected and has to be recalculated as the guided wavelength by

$$\lambda_g = \frac{v_{eff}}{f_0} = \frac{c/n_{eff}}{f_0} = \frac{1}{\sqrt{\epsilon_{eff}}}\frac{c}{f_0} = \frac{\lambda_0}{\sqrt{\epsilon_{eff}}} \tag{2.3}$$

where the refractive index, n_{eff}, is equal to $\sqrt{\epsilon_{eff}}$ and v_{eff} represents the propagation velocity in the model where the permittivity is ϵ_{eff}.

As the patch antenna can be considered a resonant cavity (Orfanidis, 2004), its effective length has to be half the wavelength (first resonance). This led us to

$$L_{eff} = \frac{\lambda_g}{2} \tag{2.4}$$

Because of the *fringing* fields, the patch's electric length is going to be bigger than its physical length. The difference between this two lengths is given by $2\Delta L$, as represented in Fig. 2.3.

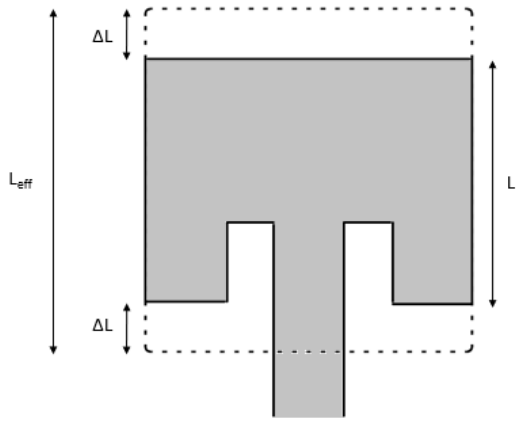

FIGURE 2.3: Difference between the electric length, L_{eff}, and the physical length, L

The difference between the two lengths is given by

$$L = L_{eff} - 2\Delta L \tag{2.5}$$

where ΔL is (Orfanidis, 2004):

$$\Delta L = 0.412h\frac{(\epsilon_{eff} + 0.3)(W/h + 0.264)}{(\epsilon_{eff} - 0.258)(W/h + 0.8)} \tag{2.6}$$

To get the final two parameters, W_i and L_i, one has first to understand why the patch has an *inset*. The *inset* is the lacking bit of metalization which makes it not rectangular, as presented before in Fig. 2.1.

If the *inset* did not exist, the impedance matching would be much more difficult. To calculate the input impedance, one needs first to calculate its reciprocal, that is, the conductance, G. The conductance captures the losses by radiation of the antenna and is determined by

$$G = \frac{W}{120\lambda_0}\left[1 - \frac{(k_0 h)^2}{24}\right] \tag{2.7}$$

where $k_0 = \frac{2\pi}{\lambda_0}$ is the wavenumber in vacuum. This equation is valid as the susceptance can be equaled to zero, $B \approx 0$, since the antenna dimensions are close to $\lambda_0/2$ (Orfanidis, 2004).

At resonance, the input resistance, R_a, is be given by

$$R_a \approx \frac{1}{2G} \tag{2.8}$$

The value of L_i is given by

$$L_i = \frac{\lambda_g}{2\pi}\arccos\left(\sqrt{\frac{R_{in}}{R_a}}\right) - \Delta L \tag{2.9}$$

where R_{in} is the input resistance (Islam et al., 2018).

The parameter W_i is empirically determined and should be more than half of the feeding width, W_{ms} (Islam et al., 2018). The reference value that is from now on used is

$$W_i = \frac{\lambda_0}{50} \tag{2.10}$$

All the equations presented in this section where introduced in a MATLAB routine where the user inputs the values of frequency, dielectric constant, height of the substrate and the desired impedance. This routine, presented in Appendix A, outputs the values of W, L, W_i and L_i.

The first and most important steps to do the design of the patch antenna are here concluded, as the next steps will be the sizing of the microstrip feed line. Its width will depend on the value of the desired impedance, as its length will depend on the phase shift.

Eq. 2.11 gives the value of a microstrip line in order to the desired height and impedance (Islam et al., 2018).

$$W_f = \frac{7.48 \times h}{e^{Z_0 \frac{\sqrt{\epsilon_r}+1.41}{87}}} - 1.25 \times t \tag{2.11}$$

where t is the copper thickness.

It is possible to easily calculate the value of W_{ms} with the software *Computer Simulation Technology – CST* (Simulia, 2022). The user inputs the initial desired definitions ($f = 2.45$ GHz, $\epsilon_r = 2.2$ and $h = 1.575$ mm) on the CST "Macros" tool, as shown in Fig. 2.4. This figure illustrates the microstrip width for a 50 Ω line.

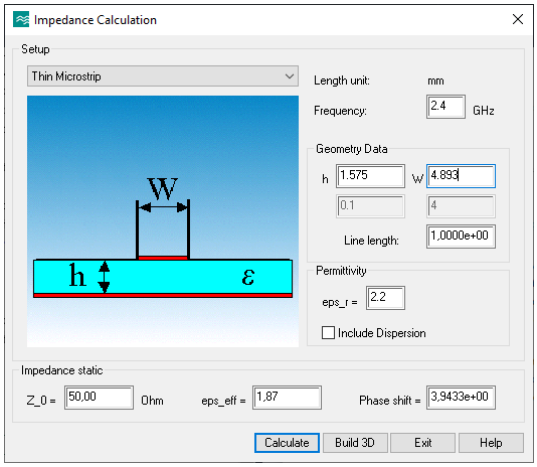

FIGURE 2.4: W_{ms} determination by CST Macro tool

Table 2.1 below shows some examples of W_{ms} values, calculated with CST Macro Tool, for different impedance lines

Impedance [Ω]	W_{ms} [mm]
50	4.893
70	2.857
100	1.417
140	0.596

TABLE 2.1: Values of W_{ms} for different impedances

The length of the microstrip, L_{ms}, will affect the phase of the patch feeding signal.

2.2 Linear Arrays

An array of antennas is a set of many single antennas combined. The benefit of using an array instead of a single element is that one is able to "direct radiated power towards a desired angular sector, depending on the number, geometrical arrangement and relative amplitudes or phases of the elements" (Orfanidis, 2004, p. 1088). By changing the phase of excitation, the main lobe can be steered to the direction desired. Furthermore, one can control the radiation pattern – main lobe as well as side lobes – with an adjustment of the magnitude of excitation currents (Tsoulos & Christodoulou, 2007, p. 532).

Uniform arrays have their elements excitation with progressive phase and constant amplitude. This type of arrays may have different geometries – linear, planar, circular or others – depending on the final goal. (Tsoulos & Christodoulou, 2007, p. 532-540).

The understanding of uniform linear arrays is the basic study of array theory, since all of its elements are displayed in a single line. Assuming, for example, a 4 element linear array and considering a far-field analysis – where $r_1 \approx r_2 \approx r_3 \approx r_4$, the total electric field observed at the observation point O in Fig. 2.5 will be given by

$$E_{total} = E_1 + E_2 + E_3 + E_4 + ... + E_N \tag{2.12}$$

With a simple manipulation, Eq. 2.12 can be rewritten as

$$E_{total} = E_1 \left(1 + \frac{E_2}{E_1} + \frac{E_3}{E_1} + \frac{E_4}{E_1} + ... + \frac{E_N}{E_1}\right) \tag{2.13}$$

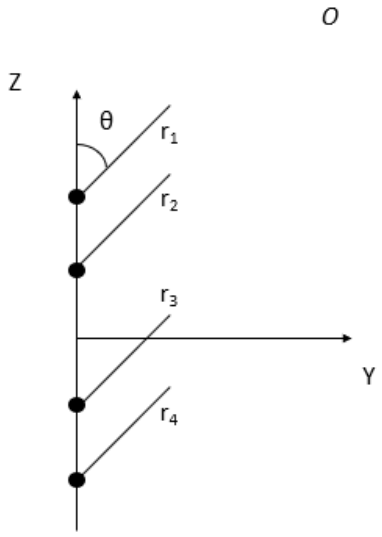

FIGURE 2.5: Far-field geometry of 4 elements (*based on Tsoulos and Christodoulou, 2007*)

As Eq. 2.13 shows, the total electric field at the observation point O can be presented by the *Element Factor* multiplied by an *Array Factor* (Orfanidis, 2004; Tsoulos & Christodoulou, 2007) where the *Element Factor* is E_1.

$$E_{total} = E_1 \times AF \tag{2.14}$$

If one considers an uniform linear array of N-elements, the array factor will be given by

$$AF = 1 + e^{j\psi} + e^{j2\psi} + e^{j2\psi} + ... + e^{j(N-1)\psi} \tag{2.15}$$

where $\psi = kd\cos\theta + \xi$, d is the distance between elements, k is the wavenumber and ξ is the phase shift. Eq. 2.15 above is a geometric series that can be simplified and normalized by

$$|AF| = \left| \frac{\sin(N\psi/2)}{\sin(\psi/2)} \right| \tag{2.16}$$

Eq. 2.16 is the array factor general equation for uniform linear arrays. This equation unveils some of the properties of an uniform linear array (Orfanidis, 2004; Tsoulos & Christodoulou, 2007):

- $|AF|$ is maximum if $\xi = 0$, that is, $\theta = \pm\frac{\pi}{2}$. This property shows that for a main lobe transversal to the array, the phase shift between elements will be null (*Broadside Array*);
- $|AF|$ is maximum if $\xi = kd \vee \xi = -kd$, that is, $\theta = \pi \vee \theta = 0$, respectively (*Endfire Array*);
- $|AF|$ is null when $\sin(N\psi/2) = 0$, that is, $N\psi/2 = \pm n\pi$ for $n = 1, 2, 3, ...$ and $n \neq N, 2N, 3N, ...$

Another very important concept of uniform linear arrays is its ***Visible Region***. The angle θ is the azimuthal angle and varies from 0^o to 180^o. Applying this property to $\psi = kd\cos\theta + \xi$, one can observe that with a simple manipulation of this expression the visible region is given by

$$-kd + \xi < \psi < kd + \xi \tag{2.17}$$

This visible region defined by the Eq. 2.17 will give us the radiation pattern interval since it depends on the frequency, distance and phase shift between elements (Orfanidis, 2004, p. 1102-1104).

So, for example, any-element broadside array that has a phase shift equal to zero, at any operation frequency and a distance between elements of $d = \lambda/2 = 62.5$ mm will have a visible region in the interval $[-kd, kd] = [-\pi, \pi]$.

Linear arrays have its elements disposed in a single axis, as shown before. By adding a second dimension, a new axis is created and it is possible to create an array with a 2D geometry. This newly created array is called a planar array since its elements are disposed on a plane. The analysis of planar arrays isn't much different from the analysis of linear arrays, since a planar array can be seen as a linear array of linear arrays (as of the array factor).

As seen before, one of the advantages of having an array is that it allows the user to direct the main beam to scan for targets. Linear arrays can do the scanning in only one polar plane – θ or ϕ –, as planar array can do it on both polar planes.

The array factor of the planar array is the multiplication of the linear array factor in the x-axis by the linear array factor in the y-axis (Tsoulos & Christodoulou, 2007, p. 537):

$$|AF|_{planar} = |AF|_x \times |AF|_y \tag{2.18}$$

By re-arranging Eq. 2.18, the normalized array factor of a N by M-elements uniform planar array is given by

$$|AF|_{planar} = \left|\frac{\sin(N\psi_x/2)}{N\sin(\psi_x/2)}\right| \times \left|\frac{\sin(M\psi_y/2)}{M\sin(\psi_y/2)}\right| \tag{2.19}$$

where $\psi_x = kd_x \sin\theta\cos\phi + \xi_x$ and $\psi_y = kd_y \sin\theta\sin\phi + \xi_y$.

2.3 Planar Array Design

As seen in Chapter 1, an antenna array will offer a higher directivity and low side lobe level compared to the one obtained by the single element. To put it in practice, the analytical formulation of an antenna array will be made in this subchapter.

2.3.1 Uniform Planar Array

Uniform planar arrays have the same spacing between elements and all of its elements have the same phase (broadside array) and magnitude excitation and can have different geometrical disposals (ex. linear, planar, circular, etc..). In this dissertation, the focus will be on planar arrays.

A linear uniform array is an array that has its elements distributed in a single axis and a planar array in two axis, as seen in Section 2.2. That said, an uniform planar array can be considered as an array of linear arrays, as demonstrated in Section 2.2.

The formulation of an uniform array of two elements, the first thing to think about is the spacing between both elements.

To start, let us assume that the spacing is half the wavelength, $\lambda_0/2$. Recalling the stand-alone element formulated in Section 2.1, the two element uniform array is presented in Fig. 2.6

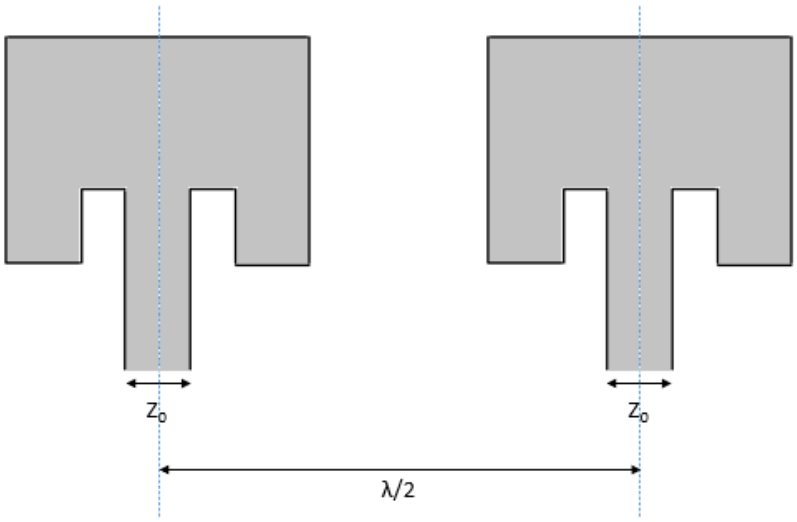

FIGURE 2.6: Linear array of two microstrip patches

And now, to formulate an uniform planar array with two elements on both axes – calling it two-by-two array –, the only thing left to do is to mirror the two element array with a spacing of $\lambda_0/2$, as shown in 2.7

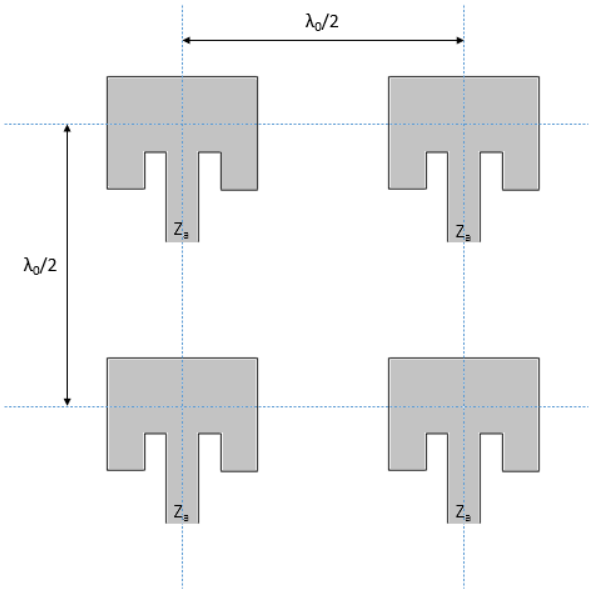

FIGURE 2.7: Example of a two-by-two planar array of microstrip patches

Note that the reference impedance (Z_0) has to be the same on all elements since it is an uniform array. This will guarantee that the excitation is the same in all of the elements.

2.3.2 Chebyshev Planar Array

Like uniform arrays, Chebyshev (and other non-uniform) arrays have the same spacing between elements. However, not all of its elements have the same excitation, according to the final goal and following the specific design rules. For a given side lobe level, one will obtain the narrowest main beam using a five-step method (Tsoulos & Christodoulou, 2007).

This type of arrays uses the Chebyshev Polynomials in terms of cosine terms. This terms are described in Tab. 2.2 (Tsoulos & Christodoulou, 2007)

$\cos 0u = 1$	$\cos 0u = 1 = T_0(x)$
$\cos 1u = \cos u$	$\cos 1u = x = T_1(x)$
$\cos 2u = 2\cos^2 u - 1$	$\cos 2u = 2x^2 - 1 = T_2(x)$
$\cos 3u = 4\cos^3 u - 3\cos u$	$\cos 3u = 4x^3 - 3x = T_3(x)$
$\cos 4u = 8\cos^4 u - 8\cos^2 u + 1$	$\cos 4u = 8x^4 - 8x^2 + 1 = T_4(x)$
$\cos 5u = 16\cos^5 u - 20\cos^3 u + 5\cos u$	$\cos 5u = 16x^5 - 20x^3 + 5x = T_5(x)$

TABLE 2.2: Chebyshev Polynomials in Terms of Cosine Terms

The Array Factor of a P-element Chebyshev array is given by Eq. 2.20 and 2.21.

$$(AF)_p = \sum_{n=1}^{M} a_n \cos\left[(2n-1)u\right] \quad \text{, for } P = 2M \text{ (even number)} \tag{2.20}$$

$$(AF)_p = \sum_{n=1}^{M+1} a_n \cos\left[2(n-1)u\right] \quad \text{, for } P = 2M+1 \text{ (odd number)} \tag{2.21}$$

where $u = (\pi d/\lambda)\cos\theta$.

The design procedure is composed by the following five steps (Tsoulos & Christodoulou, 2007):

Step 1: Replace each $\cos mu$ term in the array factor by its expansion in terms of powers of $\cos u$.

Step 2: Express the side lobe ratio R_0

$$\frac{\text{Height of the major lobe}}{\text{Height of the first side lobe}} = \frac{H_0}{H_1} = R_0$$

as a voltage ratio using

$$R_0|_{voltage} = 10^{R_0/20} \tag{2.22}$$

Step 3: Use $R_0|_{voltage}$ to determine the normalization number z_0 from

$$R_0|_{voltage} = T_{P-1}(z_0) = \cosh\left[(P-1)\cosh^{-1}(z_0)\right] \tag{2.23}$$

which yields

$$z_0 = \cosh\left(\frac{\cosh^{-1} R_0}{P-1}\right) \tag{2.24}$$

Step 4: Substitute $\cos u = z/z_0$ in the array factor of Step 1. The idea of using z_0 in the array factor is to normalize the side lobes to the value of 1.

Step 5: Equate the array factor of Step 5 to the $T_{P-1}(z)$ Chebyshev polynomial. By equating the array factor and the Chebyshev polynomial one can determine the excitation coefficients.

2.4 Feeding Network

A feeding network is composed by a set of microstrip lines that together will feed the elements of the array. At this point, the feeding network will have a feeding port.

As an example, it is important to know that a three-port power divider has to comply with the following ideal properties (Orfanidis, 2004):

- Reciprocity ($S_{ij} = S_{ji}$)
- Isolated exit ports ($S_{32} = S_{23} = 0$)
- Equal characteristic impedance in all ports
- All ports must be matched ($S_{ii} = 0$)

- Null insertion losses

Most of these properties are analysed with the *S-matrix* that describes the reflection coefficients as well as the transmission coefficients. An example of an i by j S-matrix is presented in Eq. 2.25 below

$$S = \begin{bmatrix} S_{11} & S_{12} & ... & S_{1j} \\ S_{21} & S_{22} & ... & S_{2j} \\ ... & ... & ... & \\ S_{i1} & S_{i2} & & S_{ij} \end{bmatrix} \tag{2.25}$$

where the elements contained in the matrix diagonal (where $i = j$) are the reflection coefficients, as the others are the transmission coefficients (Orfanidis, 2004).

In a transmission line, the reflection coefficients are ideally equal to zero in order to get the ports matched. This means that the energy brought through the transmission line at port 1 (at $i = 1$), for example, will not reflect on this very same port (at $j = 1$).

Since ports 2 and 3 are in parallel relatively to port 1, one concludes that the sum of the power received in ports 2 and 3 has to be equal to the power supplied by port 1. This power divider is also symmetrical (3 dB), so in the particular case where $Z_2 = Z_3$ the power is equal in both exit ports. The characteristic impedances can be easily related by

$$\frac{1}{Z_1} = \frac{1}{Z_2} + \frac{1}{Z_3} \tag{2.26}$$

The power divider can be represented by transmission lines, as shown in Fig. 2.8, where Z_{in} is the input impedance and Z_{in} is ideally equal to Z_1.

As so, the feeding network for a two element uniform antenna array will look like Fig. 2.9 and, as demonstrated by Eq. 2.26, Z_{in} will be half the impedance seen by the antennas, e.g., if $Z_{in} = 50\ \Omega$ the impedance of the lines that feed the ports (2) and (3) will be 100 Ω. Since the voltage is equal in both ports, the current is inversely proportional to the impedance.

This line of thought can be used not only for a two port divider, but for a divider with n ports, i.e., $1/Z_{in} = 1/Z_2 + 1/Z_3 + ... + 1/Z_n$.

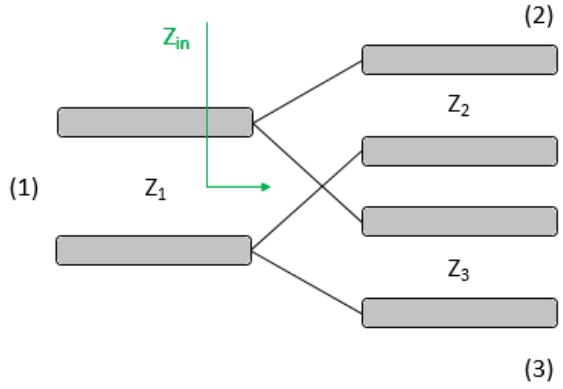

FIGURE 2.8: Power-divider with transmission lines

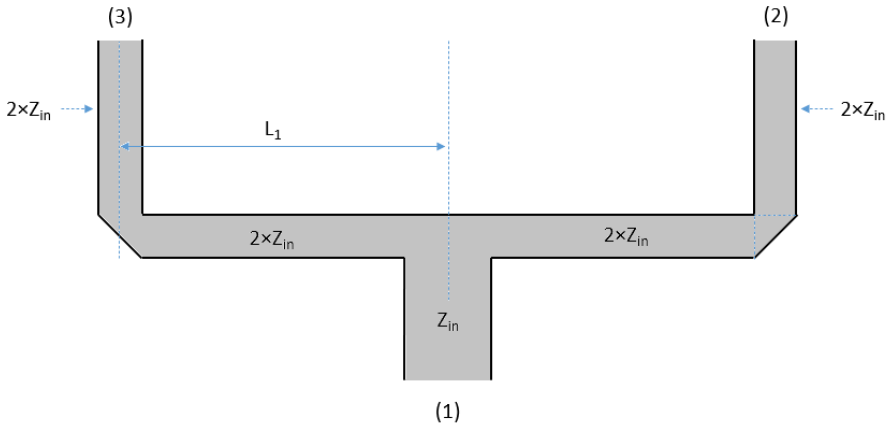

FIGURE 2.9: Power divider serving as a feeding network for a two-element array

However, there are some cases – Chebyshev arrays, for example – where the impedances of the lines that feed ports (2) and (3) are not the same. Even in these cases, all properties have to be fulfilled.

A problem that can emerge when designing a feeding network happens when two lines with different impedances are connected. This causes the impedances not to be matched. To mitigate this problem, a quarter-wave impedance transformer has to be introduced. This transformer is represented in Fig. 2.10 and Z_{in} can be calculated with Eq. 2.27 and 2.28 (Orfanidis, 2004)

$$Z_{in} = Z_{\lambda/4}\frac{Z_L + jZ_{\lambda/4}\tan(\beta l)}{Z_{\lambda/4} + jZ_L\tan(\beta l)} \tag{2.27}$$

where $Z_{\lambda/4}$ is the impedance of the quarter-wave transformer, Z_L is the load impedance, β is the wave number – $\beta = \frac{2\pi}{\lambda}$ – and l is the length of the quarter-wave

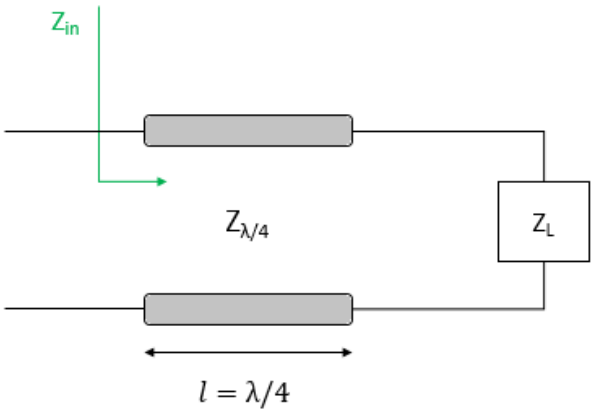

FIGURE 2.10: Quarter-wave transformer

transformer – $l = \lambda/4$.

Since $\beta l = \pi/2$, the tangents in Eq. 2.27 will tend to infinity and the complex numbers will become purely imaginary, so Z_{in} will be defined by

$$Z_{in} = Z_{\lambda/4}\frac{jZ_{\lambda/4}}{jZ_L} = \frac{{Z_{\lambda/4}}^2}{Z_L} \tag{2.28}$$

As seen before, Z_1 is ideally equal to Z_{in} and $Z_L = Z_2//Z_3$ (load impedance), so $Z_{\lambda/4}$ is deduced by

$$Z_1 = \frac{{Z_{\lambda/4}}^2}{Z_2//Z_3} \implies Z_{\lambda/4} = \sqrt{Z_1(Z_2//Z_3)} \tag{2.29}$$

and the transmission line is now represented by

A detail that one has to be cautious when formulating a quarter-wave impedance transformer is its length. $L_{\lambda/4}$ has to be the guided wavelength of the microstrip line. E.g., for $f = 2.4$ GHz, $\epsilon_r = 2.2$, $h_{sub} = 0.035$ mm and $Z_{\lambda/4} = 70\ \Omega$, ϵ_{eff} will be 1.81742 and therefore $L_{\lambda/4} = 23.2$ mm (using Eq. 2.2 and 2.3 and Tab. 2.1).

The power divider, with the quarter-wave impedance transformer, is finally represented as a microstrip line by

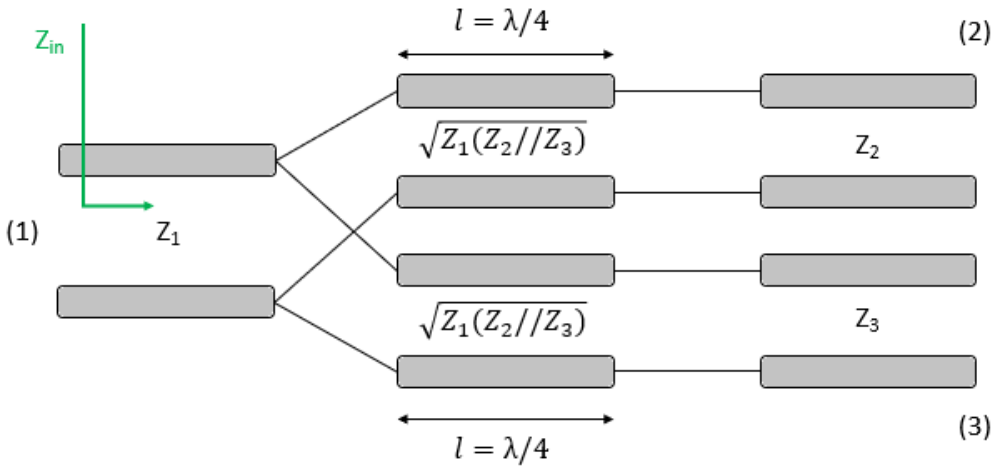

FIGURE 2.11: Power divider with the quarter-wave impedance transformer

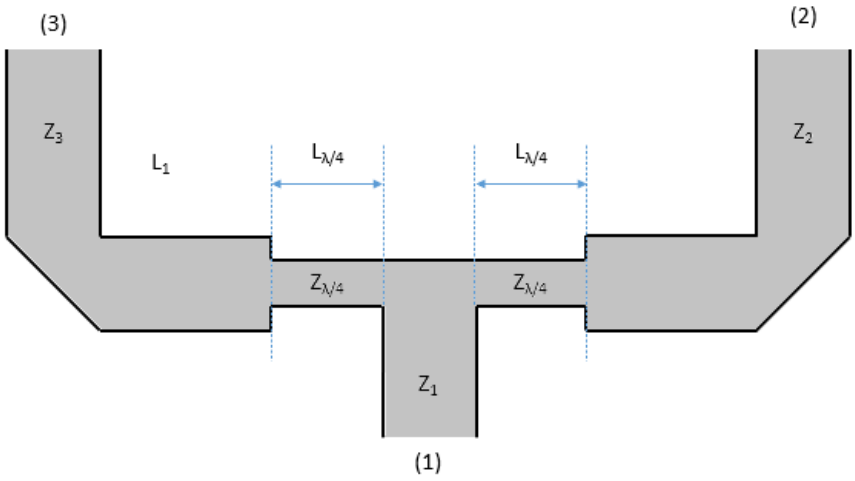

FIGURE 2.12: Power dividir with quarter wavelength transformars in microstrip line technology

Chapter 3

Numerical Simulation and Optimization of the Arrays

In this Chapter, the numerical simulation of the two four-by-four element arrays will be presented, as well as the optimization. The numerical simulation is composed by the design of the patches and feeding network in both arrays using the CST software. At the end, and after analysing the first results, the optimization of the arrays will be executed in order to obtain the desired results.

The uniform and the Chebyshev arrays will have an arrangement of four-by-four elements due to fabrication limitations: the ultraviolet exposure chamber has a limited size and the board has a dimension of 228.6x304.8 mm.

3.1 Numerical Simulation

Using the theory explored in Chapter 2, more complex arrays can be developed accordingly to the desired final goal. It is known that a planar patch array can be more or less directive, depending on the number of elements. In this chapter, a single-element will be designed, as well as two four-by-four element arrays, both spaced by $\lambda_0/2$. One will be an uniform array, as the other will be a Chebyshev array.

3.1.1 Stand-Alone Element

To simulate the antenna in CST a new project has to be created and all the calculated dimensions have to be inputed accordingly to the theory presented in Chapter 2.1. These dimensions are obtained using the MATLAB routine described in Appendix A, where the first results where obtained:

W	48.40 mm
L	40.50 mm
W_i	2.45 mm
L_i	12.37 mm

TABLE 3.1: Patch dimensions obtained in MATLAB with a feeding line of 50 Ω

Using the CST "Extrude" tool, the design of the patch, described in Fig. 3.1, is done by a list of points described below and inputed as in Fig. 3.2. The parameters L_{sub} and W_{sub} are set accordingly to Fig. 3.3

- $p_1 = \left(\frac{L}{2} + L_{ms} - L_i, 0\right)$
- $p_2 = \left(\frac{L}{2} + L_{ms} - L_i, \frac{W_{ms}}{2}\right)$
- $p_3 = \left(\frac{L}{2} - L_i, \frac{W_{ms}}{2}\right)$
- $p_4 = \left(\frac{L}{2} - L_i, \frac{W_{ms}}{2} + W_i\right)$
- $p_5 = \left(\frac{L}{2}, \frac{W_{ms}}{2} + W_i\right)$
- $p_6 = \left(\frac{L}{2}, \frac{W}{2}\right)$
- $p_7 = \left(-\frac{L}{2}, \frac{W}{2}\right)$
- $p_8 = \left(-\frac{L}{2}, 0\right)$

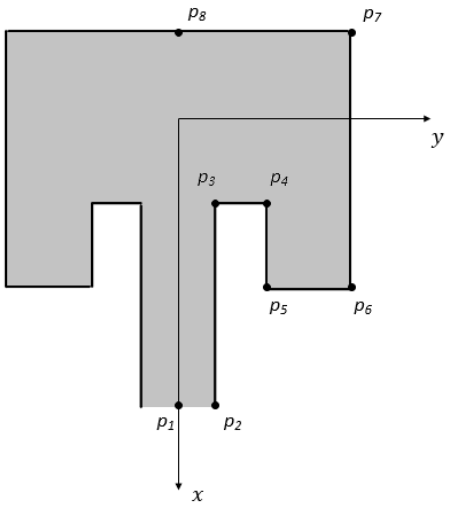

FIGURE 3.1: Interest points

Only the right-half of the patch is designed at this point, so to design the left-half of the patch one needs to mirror the image with the CST "Transform-Mirror" tool. The image is mirrored by the x-axis and then the two parts are added.

The substrate dimensions must have a margin relatively to the patch, as its height in the z-axis is already known – 1.575 mm. This margins can neither be too big or too small, so the margin dimensions are set as illustrated in Fig. 3.3.

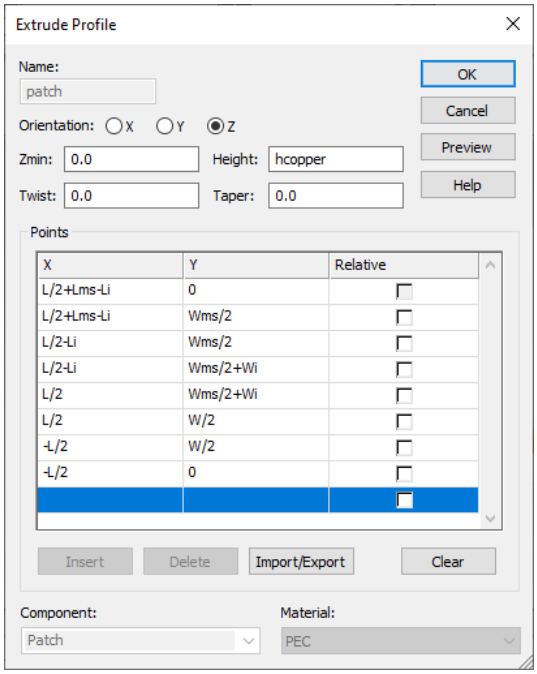

FIGURE 3.2: Interest points inputed in the "Extrude" tool

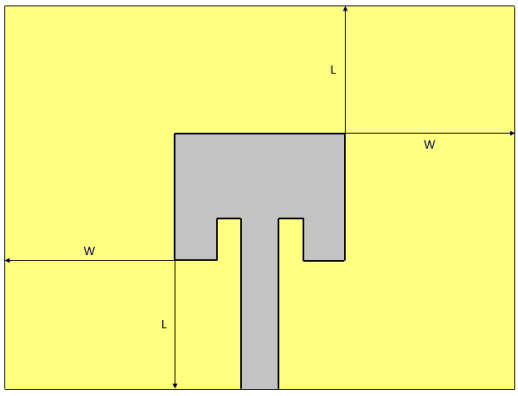

FIGURE 3.3: Margins of the substrate

The final result is shown in Fig. 3.4.

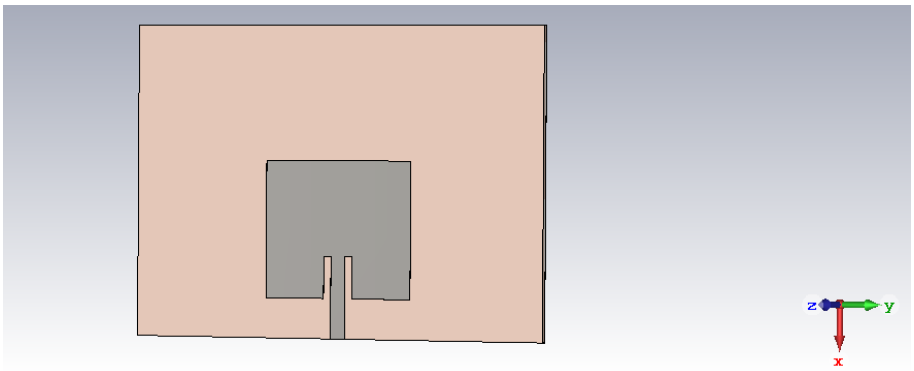

FIGURE 3.4: Patch antenna

To be able to make a simulation and analyse its features, one has to create a Waveguide Port. To do it, two faces (one in the patch and one in the ground plane) have to be selected with CST "Picks" tool, as Fig. 3.5 shows. Then, in the "Simulation" tab, the "Waveguide Port" icon is selected and the port is created.

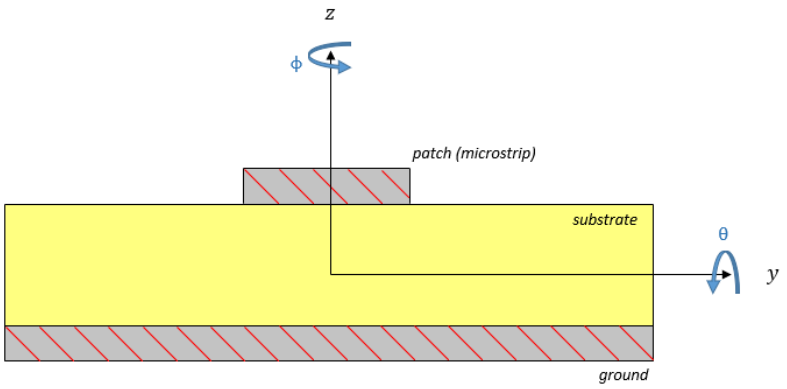

FIGURE 3.5: Waveguide port faces

Another set of data to analyse is the farfield in the desired frequency, which will be used to define the radiation pattern, directivity, gain and others. One obtains all of this data by creating a Farfield type of "Field Monitor".

The obtained amplitude of the input reflection coefficient $|S_{11}|$ in a 50 Ω characteristic impedance microstrip line is displayed in Fig. 3.6.

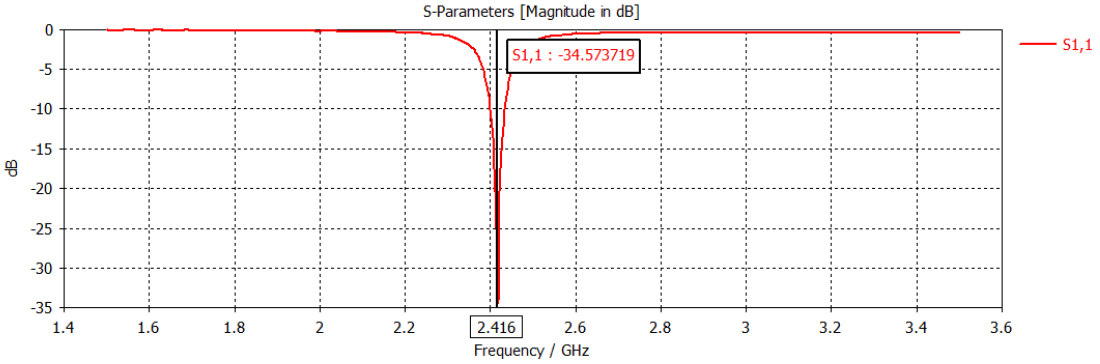

FIGURE 3.6: $|S_{11}|$ obtained in the CST simulation

As one observes, the amplitude of the $|S_{11}|$ is minimum at 2.416 GHz and is -34.57 dB. This means that the antenna is very well matched to the 50 Ω characteristic impedance but not at the desired frequency due to possible second order effects, so the patch dimensions have to be re-tuned.

As the minimum of the amplitude of $|S_{11}|$ needs to go up in frequency, the wavelength will be smaller. This thought can be utilized in the tuning of the antenna

dimensions. If one reduces the value of L by 1% and W by 8%, the $|S_{11}|$ plot will look like Fig. 3.7. These values are set empirically until the magnitude of $|S_{11}|$ is at the desired frequency.

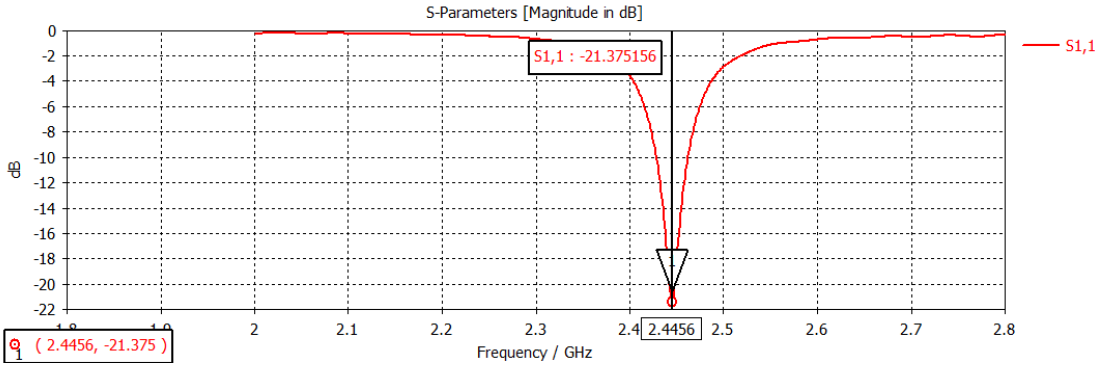

FIGURE 3.7: Matched $|S_{11}|$

The minimum value of $|S_{11}|$ is not exactly at 2.45 GHz, but this difference is small and so the antenna is considered matched at 2.45 GHz. The Smith Chart gives the two values of the impedance: the real value (resistance) and the imaginary value (reactance).

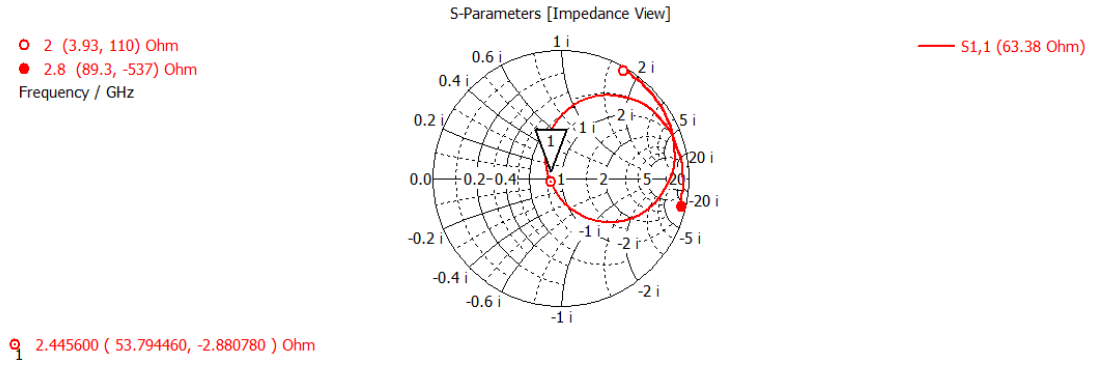

FIGURE 3.8: Smith Chart

The Smith Chart obtained is illustrated in Fig. 3.8 where both values of the impedance are represented in the bottom left corner. Once more, the difference between the obtained values and the desired 50 Ω is small.

Fig. 3.9 and 3.10 are the two dimensional polar plots of the radiation pattern. One concludes that the main lobe has the desired direction at 0° and has a side lobe level of -20.5 dB, and the magnitude of the main lobe directivity is low at 8.09 dBi in ϕ=90°. In ϕ=0°, the main lobe direction is 9° deviated with a magnitude similar to ϕ=90°, and a side lobe level of -16.0 dB.

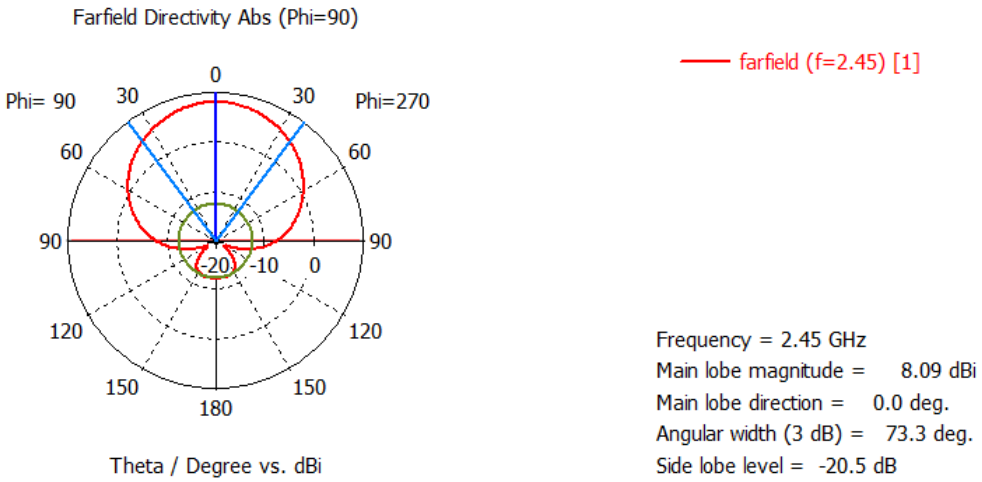

FIGURE 3.9: Radiation pattern in 2D in ϕ=90° (YZ) of a single element patch antenna

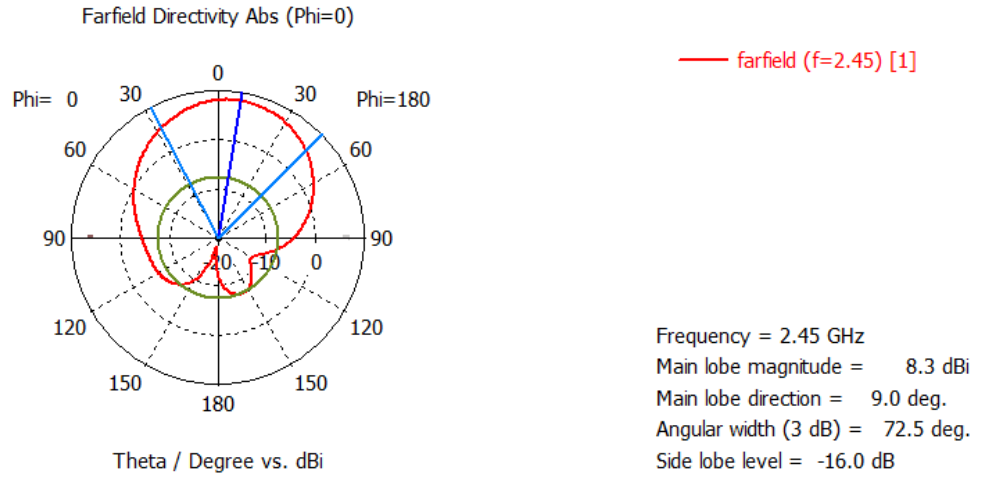

FIGURE 3.10: Radiation pattern in 2D in ϕ=0° (XZ) of a single element patch antenna

The three dimensional plot, represented in Fig. 3.11, illustrates the radiation pattern shape more clearly. This plot shows that the directivity in both planes (ϕ=90° and ϕ=0°) is similar, but with a low value for a directive antenna. The total efficiency is -0.2379 dB which corresponds to 94.7%.

An important result to analyse is the *Front-to-Back Ratio* – or *FBR*. Unlike the SLL, where the value is measured between the magnitude of the main lobe and the first side lobe, the FBR is the ratio between the amplitudes of the main lobe and the back lobe.

The FBR of the simulated antenna is approximately 25.97. Naturally, the highest the ratio, the better.

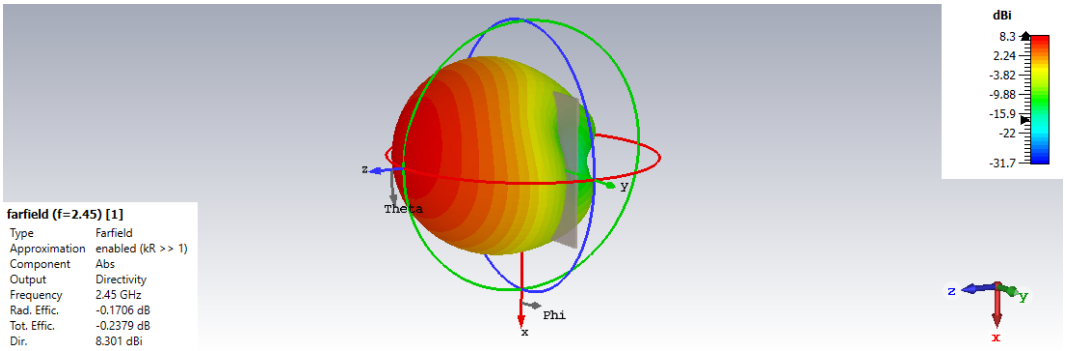

FIGURE 3.11: Radiation pattern in 3D

3.1.2 Uniform Planar Array Design

Based on the theory presented in Subsection 2.3.1 and Section 2.4, a four-by-four element array is simulated in CST. This array is designed to work at the frequency of 2.45 GHz and the distance between elements is $\lambda_0/2$.

All elements will have the same dimensions, however, the feeding network will have different impedance values. The highest impedance that one can use is 140 Ω due to the physical limitations of fabrication, since the fabrication accuracy is 0.1 mm and the width of this line is 0.596 mm. A step of 0.1 mm at this level implies a big change in the characteristic impedance.

Starting with a 140 Ω line feeding the patches, the array impedances are represented by the scheme in Fig. 3.12 and the dimensions of the patch are calculated with the MATLAB routine on Appendix A. The results of this routine are presented in Tab. 3.2.

W	48.40 mm
L	40.50 mm
W_i	2.45 mm
L_i	3.65 mm

TABLE 3.2: Uniform array patch dimensions with feeding lines of 140 Ω

However, due to the limited dimensions of the plate (228.6x304.8 mm), the parameter W has to be set to 35 mm.

The patch design scheme was substituted by dots to make an easier presentation, the orange lines are quarter-wave transformers and the red dot is where the array is fed by a 50 Ω coaxial cable. Note that the array is symmetrical, so the

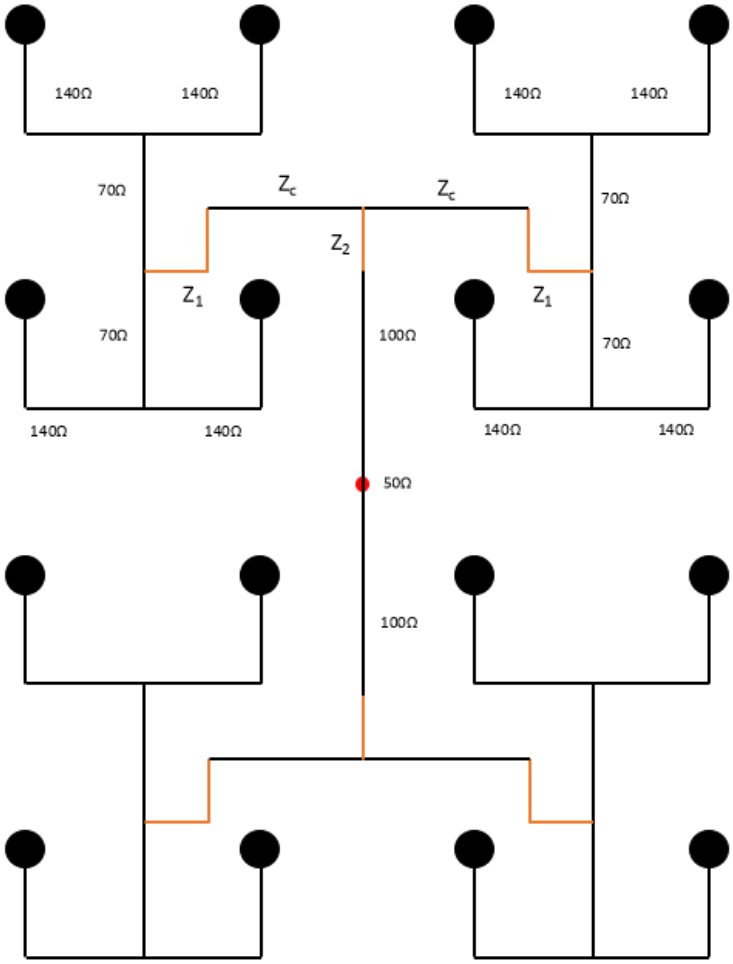

FIGURE 3.12: Uniform array feeding network scheme

bottom half will be similar to the upper half and the left half is similar to the right half.

The parallel of the two 140 Ω lines is 70 Ω, but from that point to the 100 Ω line, the impedances of Z_c, Z_1 and Z_2 have to be calculated. The way to calculate these three impedances is to set a value to Z_c. Since one wants to convert a 70 Ω line to a 100 Ω line, the intermediate value is 85 Ω and so there is not a big difference between the two impedance lines. So from now on, $Z_c = 85$ Ω and Z_1 will be

$$Z_1 = \sqrt{70//70 \times 85} = \sqrt{35 \times 85} \approx 54\ \Omega \tag{3.1}$$

and

$$Z_2 = \sqrt{85//85 \times 100} = \sqrt{42.5 \times 100} \approx 65\ \Omega \tag{3.2}$$

At this point there are many lines with different impedances, so their width has to be calculated in CST. The width of each line used in this feeding network is described in Tab. 3.3.

50 Ω	4.893 mm
54 Ω	4.358 mm
65 Ω	3.242 mm
70 Ω	2.857 mm
85 Ω	1.988 mm
100 Ω	1.417 mm
140 Ω	0.596 mm

TABLE 3.3: Characteristic impedance and width of the feeding line sections calculated in CST

As seen in Fig. 3.12, the array will be fed at the centre point of the feeding network where the impedance is 50 Ω. This is done with a coaxial cable, more specifically the EZ-86-AL, represented in Fig. 3.13, which has a 50 Ω characteristic impedance. The indicated dimensions are $d = 0.51$ mm, $D = 1.676$ mm and $g = 2.20$ mm (EZForm, 2022).

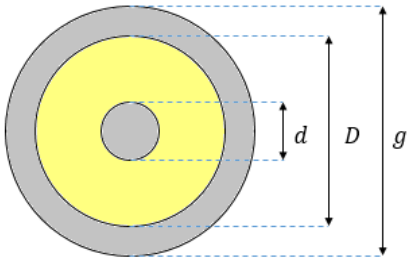

FIGURE 3.13: EZ-86-AL coaxial cable dimensions

The first step to introduce a coaxial cable to the feeding network is to make a hole that passes through the ground and substrate planes, according to the cable dimensions.

The length of the simulated coaxial cable will only have an impact on the phase shift, so the arbitrary value of 21.055 mm is chosen.

The coaxial cable used in CST is presented in Fig. 3.14 below.

At the end, a port is created to feed the coaxial line the same way other ports were created, and the coaxial cable will look like in Fig. 3.15

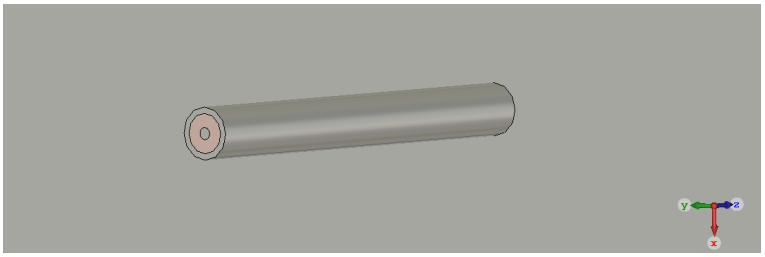

FIGURE 3.14: Coaxial line in CST

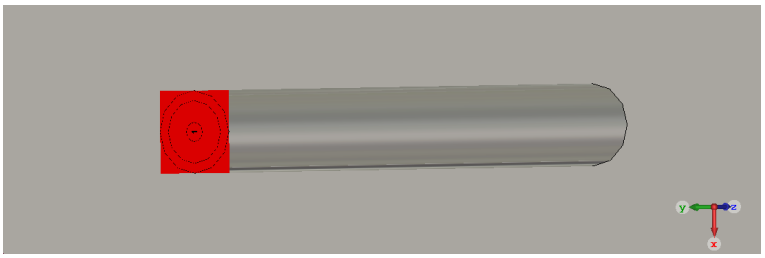

FIGURE 3.15: Coaxial port

3.1.3 Chebyshev Planar Array

Using the theory presented in Subsection 2.3.2, a Chebyshev planar array with a Side Lobe Level of -30 dB will be formulated.

Initially, four elements are disposed in a line geometry. To calculate the excitation coefficients, one uses Eq. 2.20, where P=4 and M=2 and sets the side lobe ratio to -30 dB:

Step 1: $a_1 \cos u + a_2 \cos 3u = a_1 \cos u + a_2(4\cos^3 u - 3\cos u)$

Step 2: $R_0 = 30 \implies R_0|_{voltage} = 10^{30/20} = 31.6228$

Step 3: $z_0 = \cosh\left(\frac{\cosh^{-1} R_0|_{voltage}}{P-1}\right) = 2.11745$

Step 4: $a_1 \cos u + a_2(4\cos^3 u - 3\cos u) = 4a_2 \cos^3 u + (a_1 - 3a_2)\cos u$

$(a_1 - 3a_2)\frac{Z}{Z_0} + 4a_2(\frac{Z}{Z_0})^3 = (\frac{4a_2}{Z_0^3})Z^3 + (\frac{a_1-3a_2}{Z_0})Z$

Step 5: Using $T_3(Z) = 4Z^3 - 3Z$ and equaling

$4Z^3 - 3Z = (\frac{4a_2}{Z_0^3})Z^3 + (\frac{a_1-3a_2}{Z_0})Z$

And creating a system of equations

$$\begin{cases} \frac{4a_2}{Z_0^3} = 4 \\ \frac{a_1-3a_2}{Z_0} = -3 \end{cases} \implies \begin{cases} a_1 = 22.129 \\ a_2 = 9.49378 \end{cases}$$

The excitation coefficients, a_1 and a_2, determine the ratio of the amplitude supplied to each element. The goal of a Chebyshev array is to have a directive main lobe and a low side lobe level, so in a four element array the two middle elements will have to receive $a_1/a_2 = 2.33$ times the amplitude received by the two elements in the edges, as Fig. 3.16 shows.

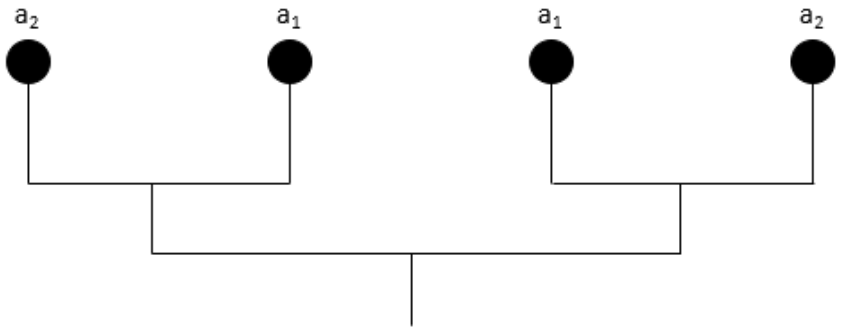

FIGURE 3.16: One-by-four Chebyshev array

In order to feed the the elements with different powers, the lines of the feeding network must have different impedances. Those impedances have to comply with the 2.33 ratio defined by the Chebyshev excitation coefficients, so the impedance of the line that feeds the middle elements will have to be 2.33 times smaller than the others.

Due to the limitation of manufacturing, the maximum accepted impedance line has 140 Ω. Therefore, the lines that feed the edge elements will have 140 Ω and the middle elements will have lines of 60 Ω. Using Eq. 2.26, where Z_2 is 140 Ω and Z_3 is 60 Ω, the points (1) and (2) where the two impedance lines touch will have 42 Ω (Z_1).

The array will be fed by a 50 Ω line, as Fig. 3.17 shows. This line will divide itself in two lines of 100 Ω to comply with Eq. 2.26. At this point, the two 100 Ω lines will encounter the 42 Ω points. This creates a non-matched feeding network, so a quarter-wave transformer has to be introduced between this lines.

Using Eq. 2.29, where Z_1 is 100 Ω, Z_2 is 140 Ω and Z_3 is 60 Ω, $Z_{\lambda/4}$ will be approximately 65 Ω. Now, using Eq. 2.2 and 2.3, the length of the quarter-wave impedance will be 22.6 mm. The array will look like in Fig. 3.17.

To design a four-by-four element array one repeats the process in the x and y-axis, always respecting the determined 2.33 ratio, as presented in Fig. 3.18. In this figure, the dimensions are only presented on the right side to make the presentation easier. The left side will be equal.

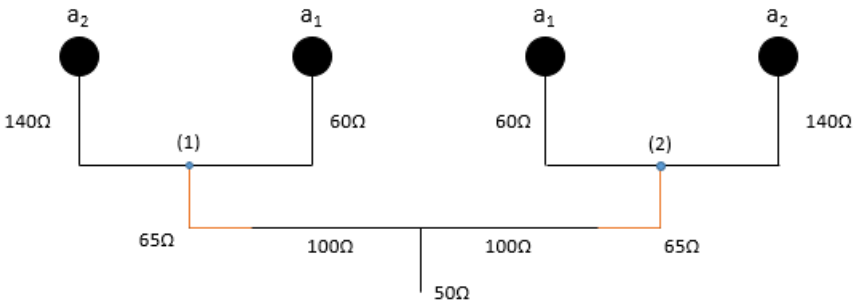

FIGURE 3.17: One-by-four Chebyshev array scheme

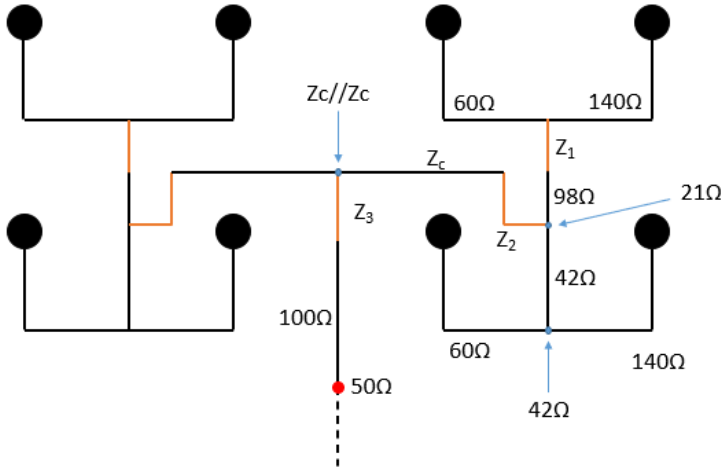

FIGURE 3.18: Sizing of a four-by-four Chebyshev array

The 42 Ω line is easily defined by the parallel of the 140 Ω and 60 Ω lines. Multiplied by the 2.33 ratio, one obtains the 98 Ω line. However, the 98 Ω line is not matched with the parallel of the lines above, so a quarter-wave transformer has to be introduced (Z_1). Using Eq. 2.29, Z_1 is $\sqrt{98(60//140)} = 64$ Ω.

The parallel of the 42 Ω and 98 Ω lines is 21 Ω, which is a very wide line. At this point, one has to define Z_c in order to find Z_2 and Z_3. Z_c does not have a method to be defined, so one defines Z_c as 70 Ω.

According to Eq. 2.29 and considering that Z_c is 70 Ω, Z_2 is equal to $\sqrt{70(98//42)} = 45$ Ω. The parallel of the two lines with the Z_c impedance is calculated with Eq. 2.26 and is 35 Ω.

Once again, $Z_c//Z_c$ is not matched with the 100 Ω line, so another quarter-wave transformer has to be introduced (Z_3). Using Eq. 2.29, Z_3 is $\sqrt{100(70//70)} = 59$ Ω.

The list with all the impedance values and their width is presented in Tab. 3.4.

42 Ω	6.285 mm
45 Ω	5.702 mm
50 Ω	4.893 mm
59 Ω	3.797 mm
60 Ω	3.698 mm
64 Ω	3.327 mm
70 Ω	2.857 mm
98 Ω	1.481 mm
100 Ω	1.417 mm
140 Ω	0.596 mm

TABLE 3.4: Characteristic impedance and width of the feeding network lines in a four-by-four Chebyshev array

A detail that one has to consider is the fact that the array is mirrored from the left half to the right half and also from the upper half to the lower half.

The same coaxial cable used in the Uniform Array is used in this array as well. The full four-by-four array scheme is presented in Fig. 3.19.

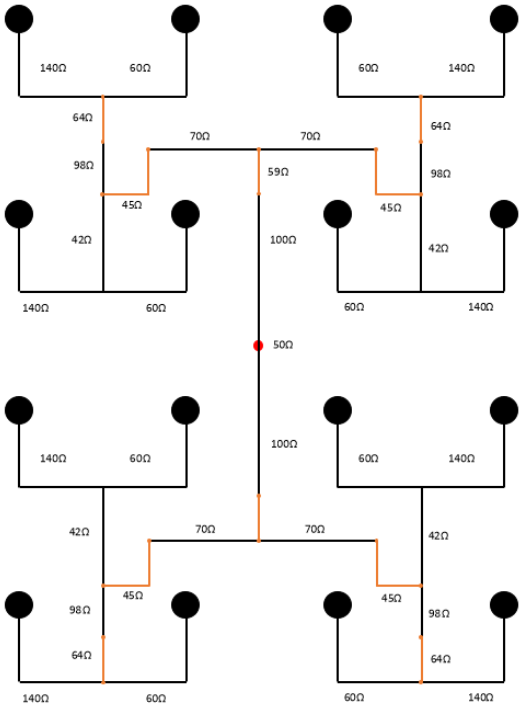

FIGURE 3.19: Four-by-Four Chebyshev array scheme

3.2 Optimization

Both arrays designed in the last section are not optimized. The theoretical calculations to design the arrays does not contemplate the existing losses or any other second order side effects, such as coupling between patches and between lines, that can influence the desired result.

Therefore, the arrays have to be optimized in some aspects such as dispersion, the lengths and widths or even the spacing between elements. Some new line designs will be implemented as well in order to mitigate some of the effects.

3.2.1 Uniform Planar Array

The uniform array with the coaxial cable simulated in CST is presented in Fig. 3.20. This array is not optimized since there are still some characteristics that can be improved.

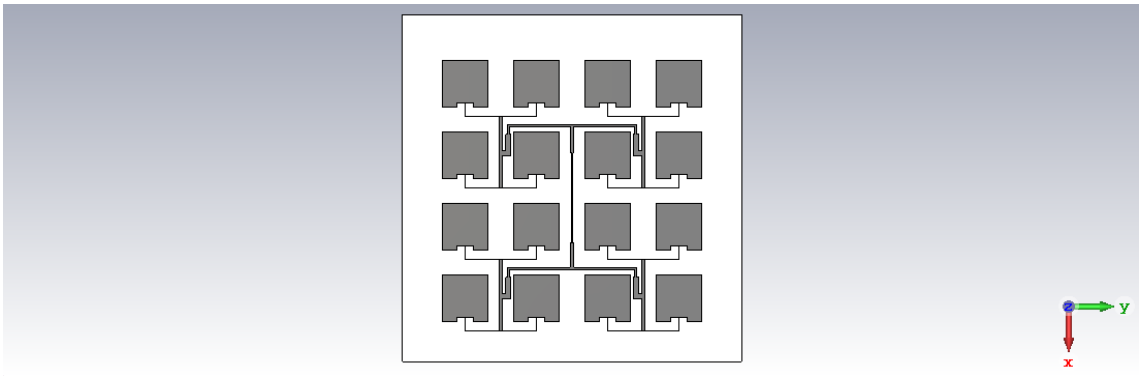

FIGURE 3.20: Non-optimized uniform array designed in CST

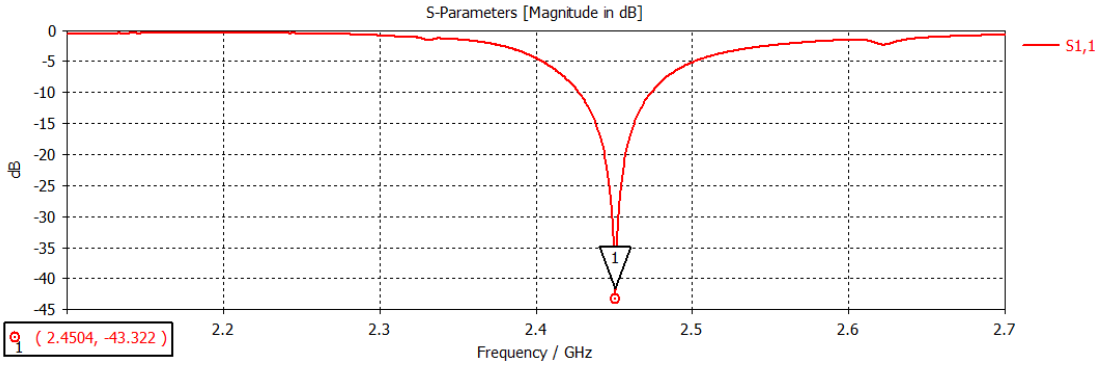

FIGURE 3.21: Magnitude of $|S_{11}|$ before optimization

The $|S_{11}|$ magnitude is approximately at 2.45 GHz and the real and imaginary values of the array input impedance are very close to the desired ones, as

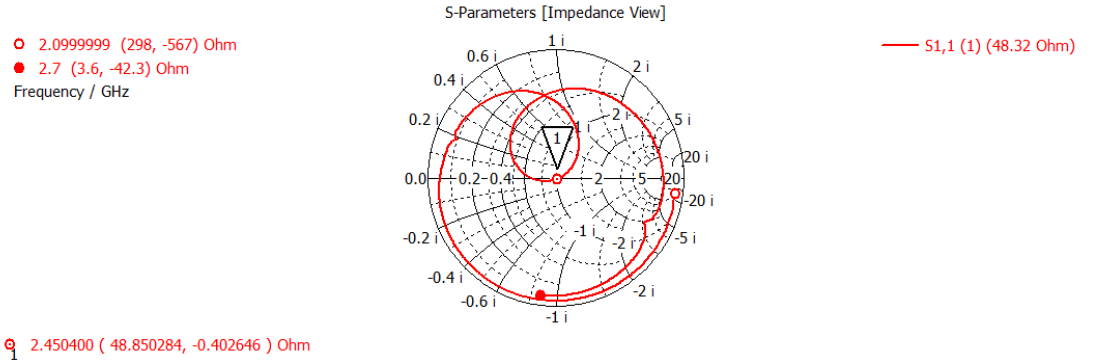

FIGURE 3.22: Magnitude of $|S_{11}|$ before optimization

presented in Fig. 3.21 and 3.22. These are excellent results that don't need to be optimized.

The 2D plot of the radiation pattern is presented in Fig. 3.23.

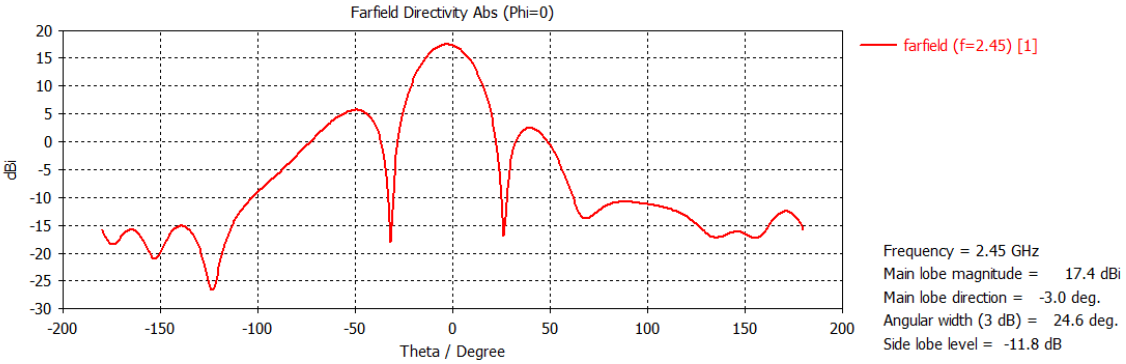

FIGURE 3.23: Radiation pattern of the uniform array before tuning in ϕ=0°

The side lobe level, now at -11.8 dB, is improved by making an fine tuning in some parameters. This fine tuning is an empiric process, where the parameters tuned were L by 99.5% and W_i by 60%. By tuning the parameter L, the $|S_{11}|$ minimum magnitude will slide to upper frequencies, so a balance has to be found between the optimization of the radiation pattern and the magnitude of $|S_{11}|$.

The tuning made the side lobe level to be smaller and better than it was before and is now -12.3 dB, as Fig. 3.24 shows.

To improve even more the side lobe level, an island is inserted on the connection between the 50 Ω and the 100 Ω lines. The difference between impedances at this point is very big, so the island will reduce this problem. The island is represented in Fig. 3.25.

The side lobe level in ϕ=90° is at -15.2 dB, which is already a good result.

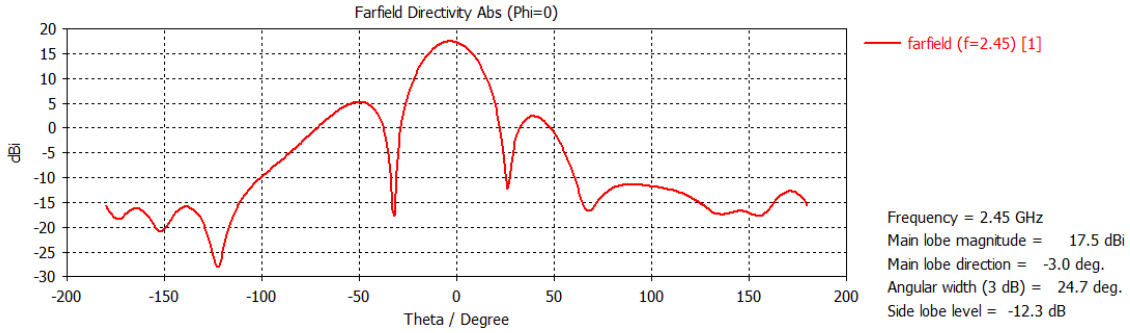

FIGURE 3.24: Radiation pattern of the uniform array after tuning in ϕ=0°

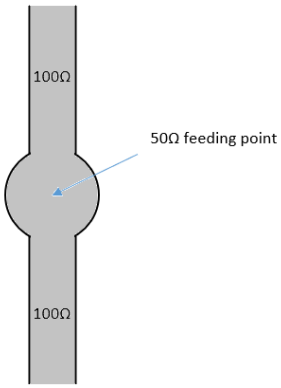

FIGURE 3.25: Island at the middle point between the 50Ω and the 100Ω lines

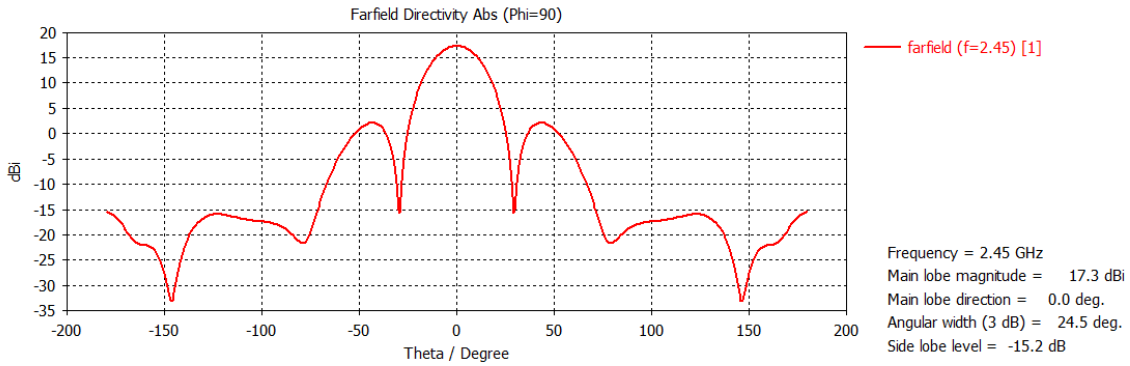

FIGURE 3.26: Radiation pattern of the uniform array in ϕ=0°

The directivity is now at 17.42 dB, as Fig. 3.27 shows. This aspect can be improved by tuning the spacing between elements.

At this point, the spacing between elements is $\lambda_0/2$, or 61.2245 mm. The elements are moved away from each other by another 4.4 mm, which corresponds to 7.2%, so the final distance between them is 65.625 mm. The array is once again simulated and the radiation pattern is presented in Fig. 3.28.

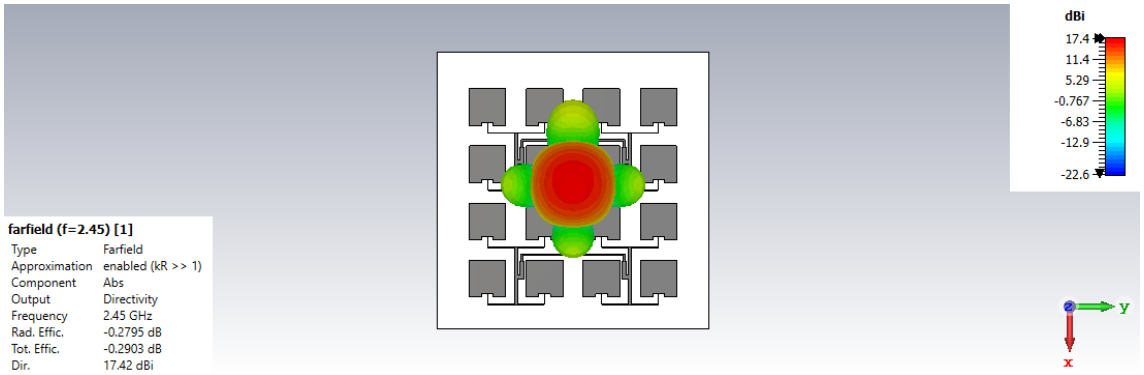

FIGURE 3.27: Radiation pattern of the uniform array in 3D

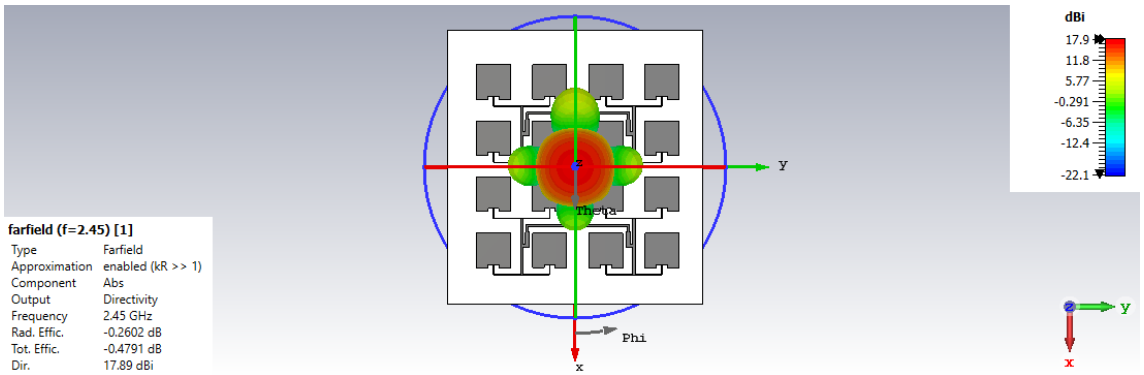

FIGURE 3.28: Radiation pattern of the optimized uniform array in 3D

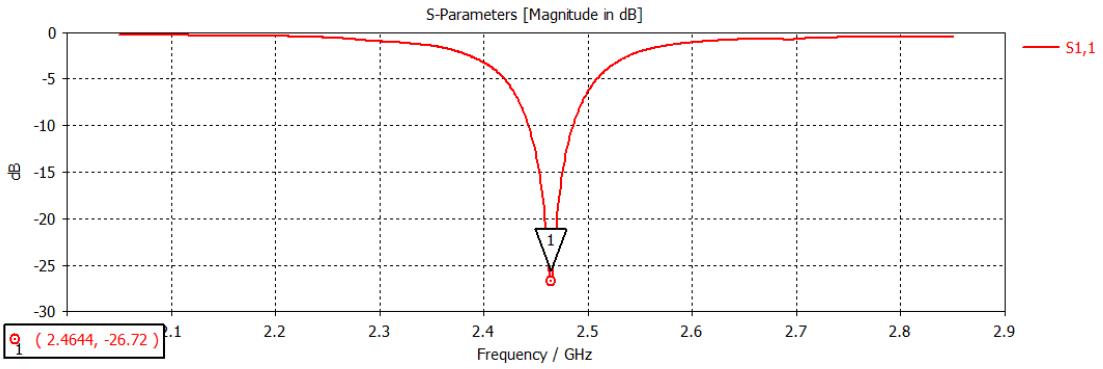

FIGURE 3.29: Optimized magnitude of $|S_{11}|$

The lowest magnitude of the $|S_{11}|$ is now at 2.4644 GHz, as presented in Fig. 3.29, which means that the array is not matched exactly at 2.45 GHZ as it was before. However, the difference is small, so this result is accepted. The compromise between the optimization of the radiation pattern and the minimal amplitude of $|S_{11}|$ was fulfilled. As to the Smith Chart, the results show a difference on the real value of the impedance, but not a significant one.

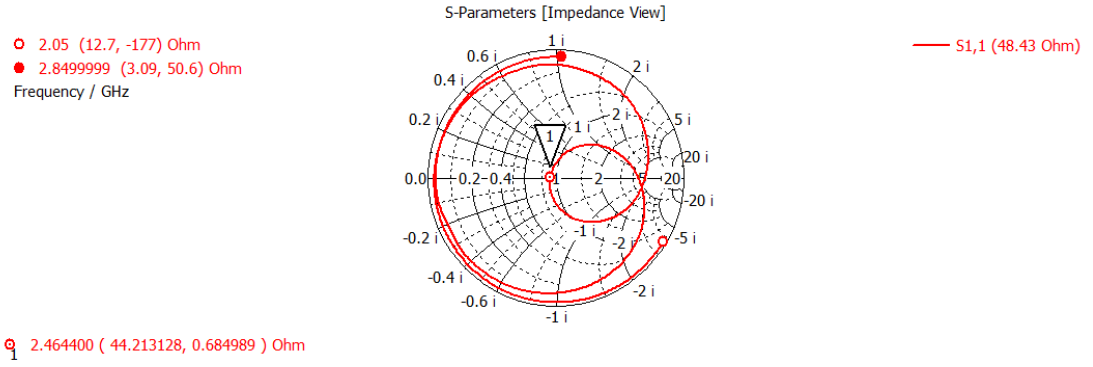

FIGURE 3.30: Optimized magnitude of $|S_{11}|$

The radiation pattern plot in 2D, presented in Fig. 3.31 shows that the side lobe level has decreased in ϕ=0°.

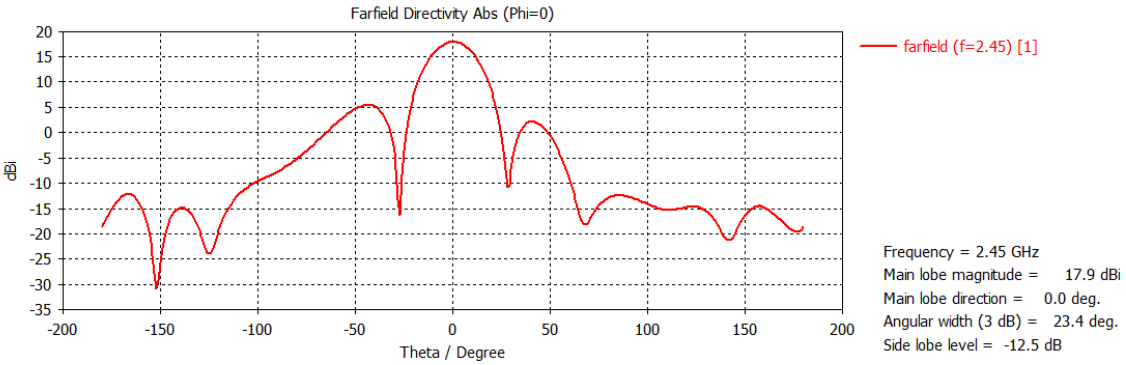

FIGURE 3.31: Radiation pattern of the optimized circuit in ϕ=0°

The side lobe level in ϕ=90° has increased by 0.6 dB. This value is acceptable since -14.6 dB is still greater than the -13.5 dB.

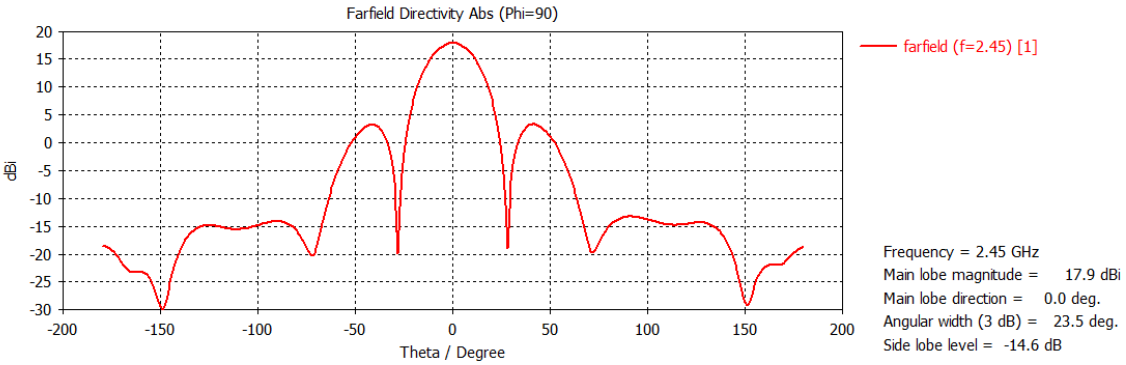

FIGURE 3.32: Radiation pattern of the optimized circuit in ϕ=90°

3.2.2 Chebyshev Planar Array

The non-optimized Chebyshev array is presented below in Fig. 3.33.

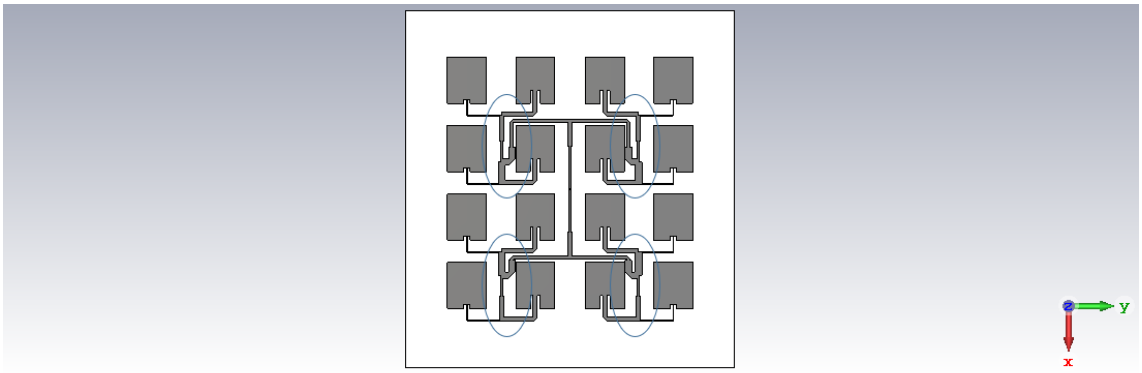

FIGURE 3.33: Non-optimized Chebyshev array in CST

As one observes, there are several aspects that have to be tuned and/or optimized. The first obvious thing that can be improved is the fact that the lines of 64 Ω, 98 Ω and 42 Ω are very close to the elements, as signalized in Fig. 3.33. This causes second order effects, specially parasitic capacitance effect, that can influence the results. To reduce this effect, the lines have to be moved to the middle of both elements in the y-axis, as Fig. 3.34 shows.

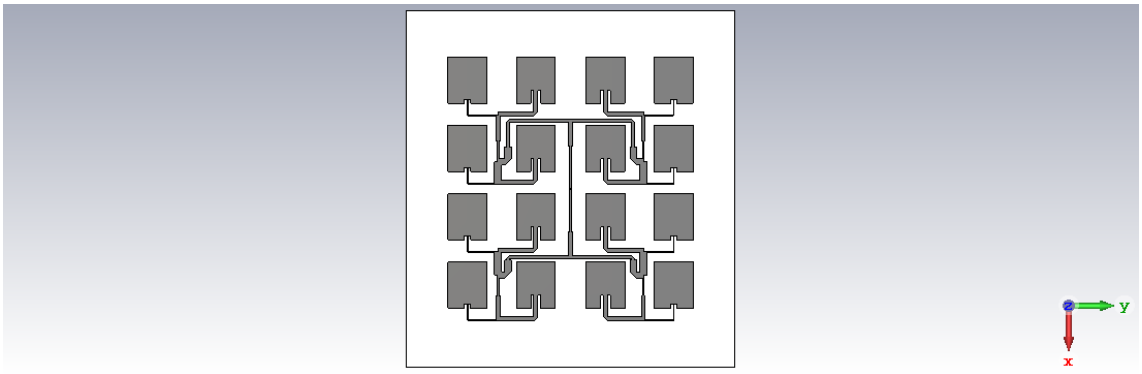

FIGURE 3.34: Repositioning of the vertical lines between elements in the x-axis

Observing Fig. 3.34, one notices that the upper horizontal lines of 70 Ω are very close to the second row elements, so all the horizontal lines are moved up by 0.875 mm.

The second main feature that has to be redesigned is the electrical length of the 140 Ω and 60 Ω lines so that all of the elements are in phase. The electrical length is calculated with Eq. 2.2 and 2.3, so $\lambda_{g1} = 93.78$ mm and $\lambda_{g2} = 90.21$ mm.

Fig. 3.35 shows a scheme of the 140 Ω and 60 Ω lines, where the variables a, b, c and d represent the lengths of the lines. In order to calculate the electrical length, and since the 60 Ω line is wider than the 140 Ω, the 60 Ω will have a fixed

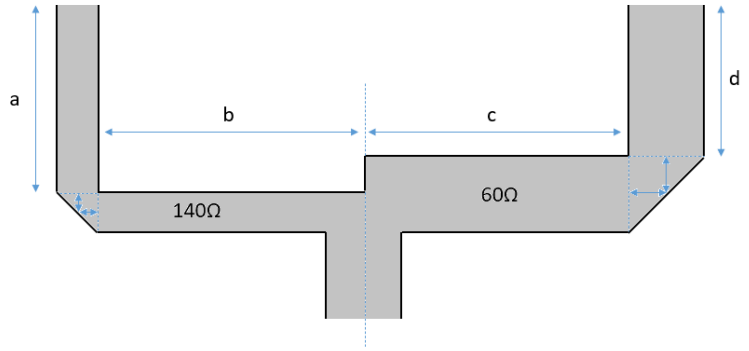

FIGURE 3.35: 140 Ω and 60 Ω lines with different electrical lengths before being redesigned

length. That is, the values of the variables c and d are fixed. The value of the variable a is also fixed in order to make an easier redesign, since only one variable will be unknown. Measured the distances, $a = 13.4975$ mm, $c = 32.1416$ mm and $d = 18.2369$ mm.

As means to get equal electrical lengths in both lines, one deducts Eq. 3.3.

$$\frac{L_1}{\lambda_{g1}} = \frac{L_2}{\lambda_{g2}} \implies \frac{L_1}{L_2} = \frac{\lambda_{g1}}{\lambda_{g2}} = 1.03962 \tag{3.3}$$

where $L_1 = a + b + W140$ and $L_2 = c + d + W60$. As so,

$$\frac{L_1}{L_2} = \frac{a + b + W140}{c + d + W60} = \frac{b + 14.0935}{54.0745} \tag{3.4}$$

The variable b is easily discovered by

$$\frac{b + 14.0935}{54.0745} = 1.03962 \implies b = 42.1\ mm \tag{3.5}$$

The original value of b ($b_{original}$) was 26.9369 mm, which is significantly smaller than the calculated b. The elements have to maintain the same horizontal distance between them, but the horizontal part of the 140 Ω line (b) has to be much bigger. To overcome this problem, a new design of this line is made.

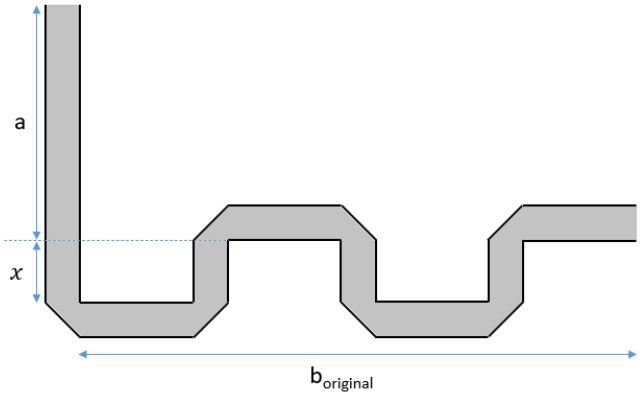

FIGURE 3.36: Redesigned line of 140Ω

The new design of this line is presented by the scheme in Fig. 3.36. The length of the 140 Ω (L_1) is 56.2169 mm, accordingly to Eq. 3.4 and 3.5. As illustrated in Fig. 3.36, this length is now be defined as

$$L_1 = a + b_{original} + 4 \times W140 + 4x \tag{3.6}$$

And so the value of x is easily discovered. In order to get the desired electrical length in this line, the value of x is 3.3 mm.

To test if the elements are being fed at the same phase, all the elements are removed and discrete ports are added with the respective impedance value. An island with a radius of 1.1 mm is also added at the middle of the 100 Ω line to avoid the big impedance difference between this line and the 50 Ω coaxial line.

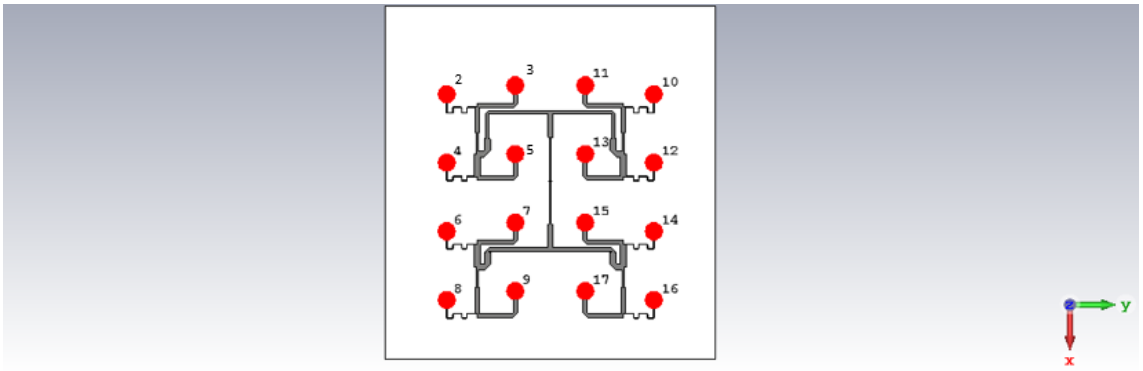

FIGURE 3.37: Removal of all the elements and input of discrete ports in the feeding network

Fig. 3.37 shows the feeding network without the elements and with the discrete ports inserted. As one observes, the even numbered ports correspond to the

140 Ω lines, while the odd ports correspond to the 60 Ω lines (port 1 is the feeding port at the coaxial cable).

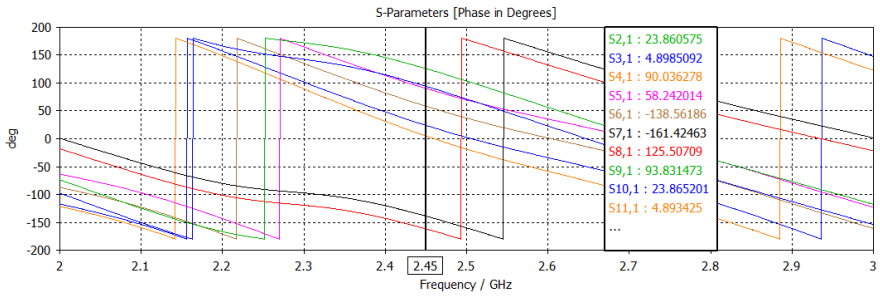

FIGURE 3.38: Phase of each port after the first simulation

The results of the simulation show that the ports are out of phase, as presented in Fig. 3.38.

Dividing the ports in pairs (2-3, 4-5, 6-7 and 8-9), and looking at the phase of the pair 2-3, there is a difference of about 19°. To avoid that big of a difference, the value of x is empirically set to 4.5 mm. All of the other pairs of ports are optimized the same way. For the pair 4-5, $x = 5.6$ mm, the pair 6-7 has a value of $x = 4.6$ mm and the pair 7-8 has a value of $x = 5.6$ mm. All the elements are now in phase with their respective pair. Note that the right half of the circuit is symmetric to the left half.

The results are shown in Fig. 3.39.

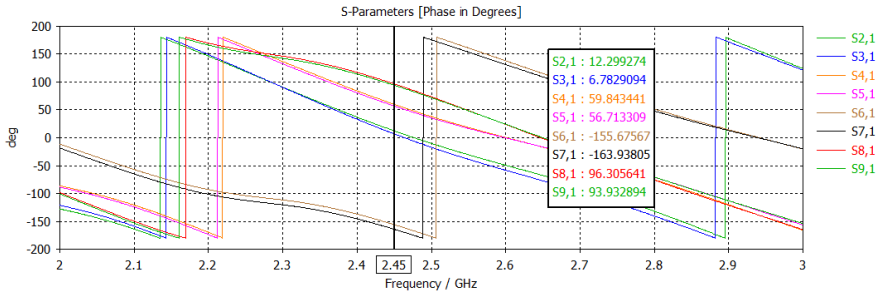

FIGURE 3.39: Phase of ports 2 to 9 after tuning

Now the pairs are in phase. There are some small differences between phases, but these differences are acceptable.

The next step is to get the pairs in phase with each other. To do so, the points were the 45 Ω line joins with the 98 Ω and 42 Ω lines have to be tuned, as well as the feeding point. These points can be lowered or raised in order to get the phases aligned.

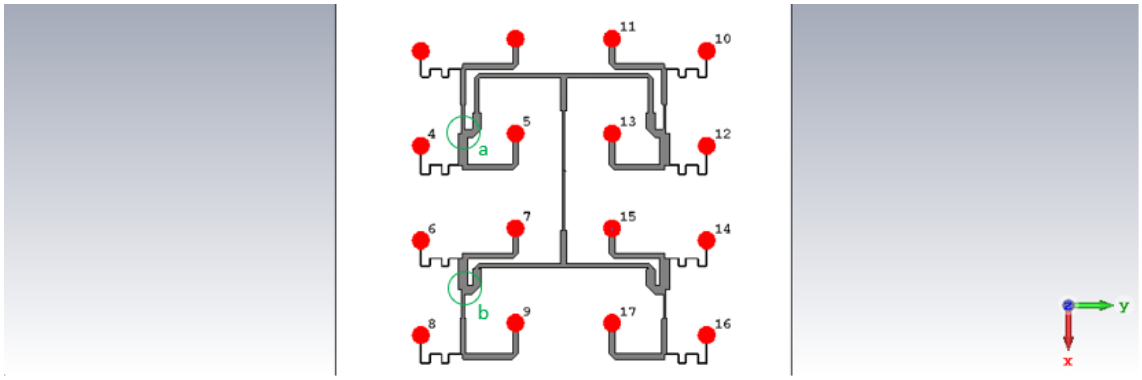

FIGURE 3.40: Points were the lines have to be tuned

This points a and b, represented in Fig. 3.40, are tuned by -5.8 mm and -13.7 mm, respectively. The feeding point is also tuned by -0.4 mm. Now the phases of all elements are aligned (with some small differences), as Fig. 3.41 shows.

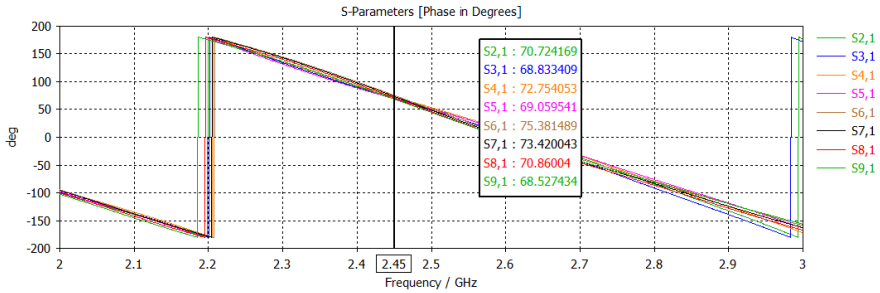

FIGURE 3.41: Element phases after tuning

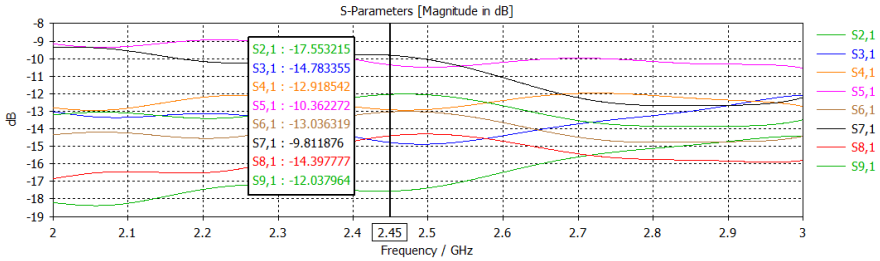

FIGURE 3.42: Element magnitudes in dB

The magnitudes of the power fed to the elements are represented in Fig. 3.42. To improve the Chebyshev ratio of 2.33, the parameter L is set to 97.5% of its original value and W_i is set to 70% of its original value. The width of the 42 Ω line is also increased by 30%. The radius of the island projected at the feeding point is also increased to 4.5 mm. The tuned magnitudes of the elements, as presented in Fig. 3.43, show some improvement but not as desired. The Chebyshev ratio of 2.33 is still not fulfilled.

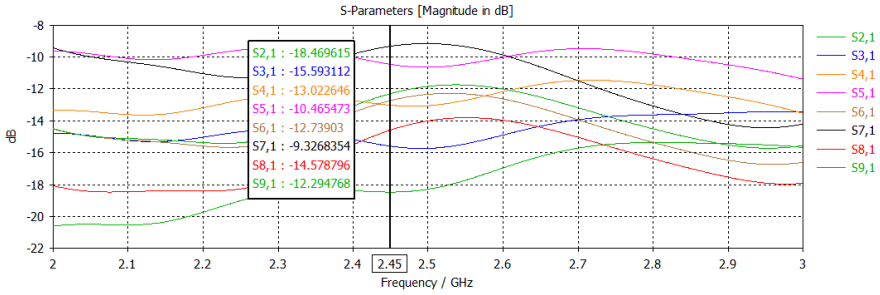

FIGURE 3.43: Tuned magnitudes

Added the elements to feeding network and removing the discrete ports, the final Chebyshev antenna is presented in Fig. 3.44.

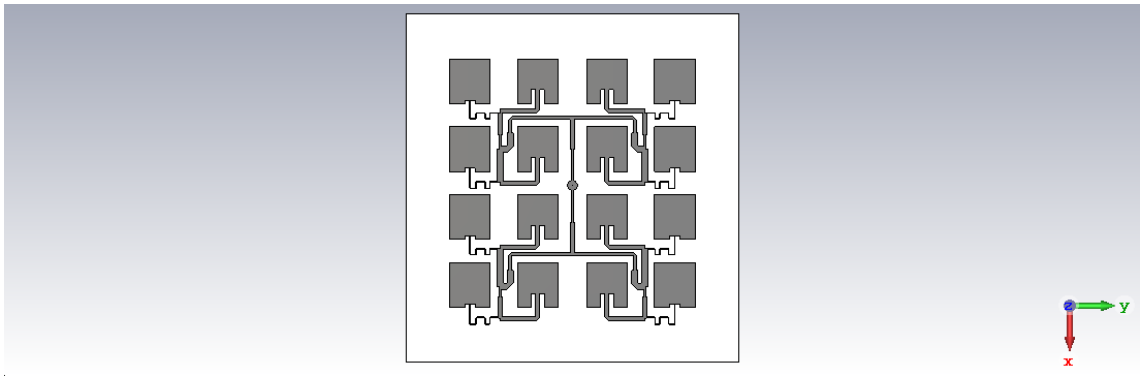

FIGURE 3.44: Final Chebyshev circuit

After simulating the complete circuit, the magnitude of the $|S_{11}|$ parameter is at the desired frequency, as Fig. 3.45 shows.

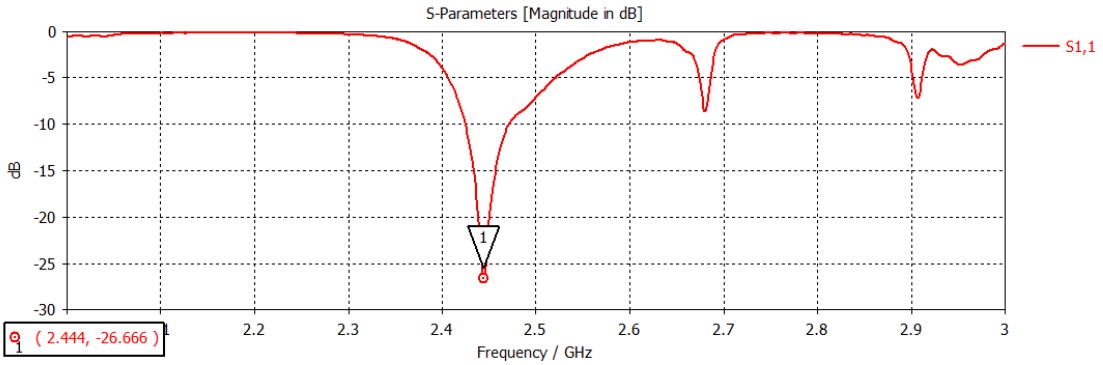

FIGURE 3.45: Final Chebyshev $|S_{11}|$

The values of the real and the imaginary parts of the impedance are also good, as presented in Fig. 3.46.

As to the radiation pattern, the 3D plot is presented in Fig. 3.47. The directivity is now at 17.30 dBi with a total efficiency of 93.3%.

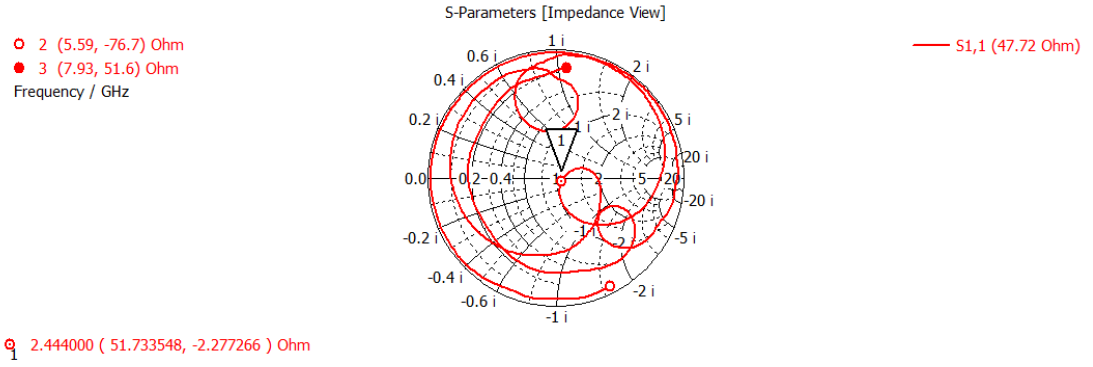

FIGURE 3.46: Final Chebyshev Smith Chart

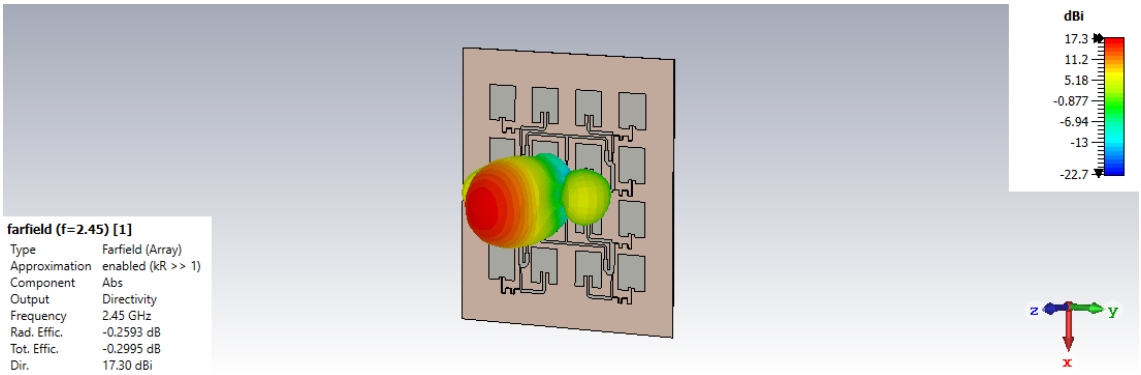

FIGURE 3.47: Final Chebyshev 3D radiation pattern

The radiation pattern in 2D is presented in Fig. 3.48 and 3.49 being the ϕ=0° and ϕ=90° cuts, respectively. As shown by these results, the side lobe level is not being fulfilled as desired.

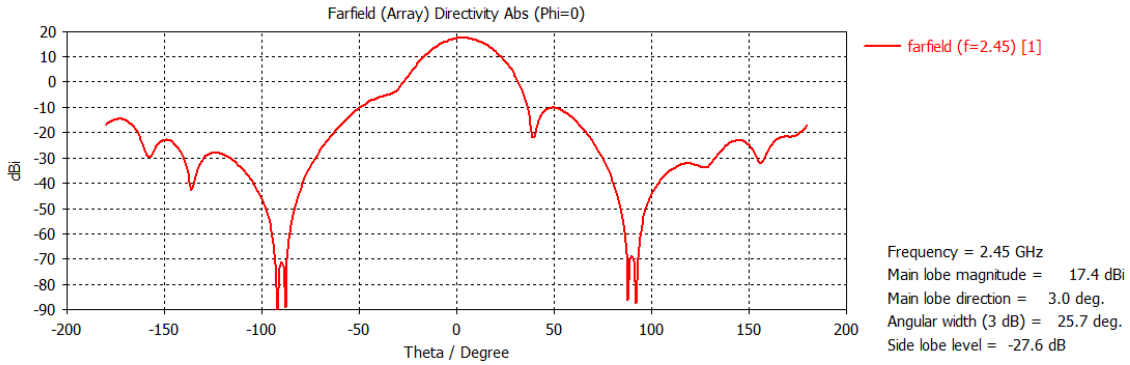

FIGURE 3.48: Final Chebyshev 2D radiation pattern at ϕ=0°

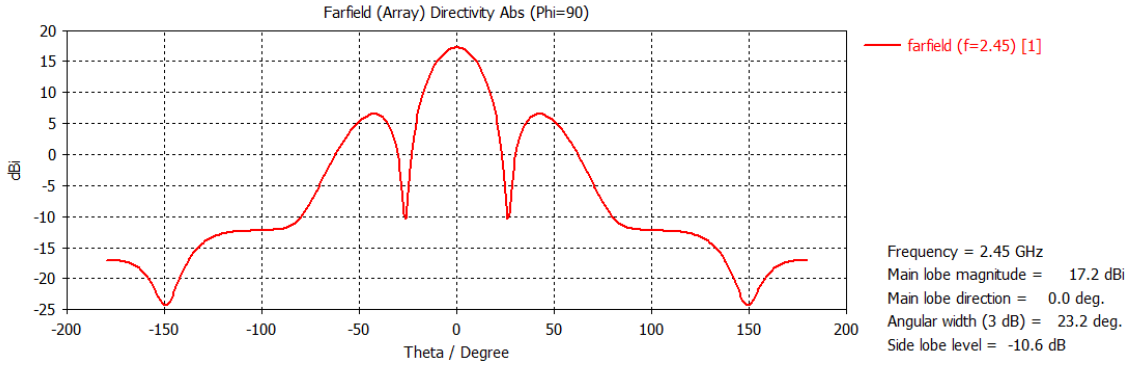

FIGURE 3.49: Final Chebyshev 2D radiation pattern at ϕ=90°

Chapter 4

Experimental Validation

4.1 Prototype Fabrication

To fabricate both prototypes, one has to follow the eight steps tutorial presented below:

Step 1: Pre-treatment of the material

The surface to be sprayed must be absolutely grass free. To ensure this, the surface must be cleaned with a good detergent. The detergent is rubbed with a moist rag so that it brightens the copper surface, removes any oxides and makes the copper layer completely wettable. After rinsing the plate thoroughly, it is dried between sheets of absorbent paper taking extreme care to avoid any fingerprints on the board surface. Abrasive pads or solvents should not be used to clean the surface.

Step 2: Application of layer

This part has to be done in a subdued light and dust-free environment. The board should be placed in a horizontal position and the spray (Positiv 20) applied from a distance of approximately 20 cm from the board. To give an uniform distribution, the application of the spray should be made in serpentine lines. The application of too much spray will result in undesired edges and coats of varying thickness requiring longer exposure time. Whilst spraying, the can should be held in a vertical or slightly inclined position and afterwards the board should not be exposed to daylight.

Step 3: Drying

After application of the sprayed-on coating, the board must be dried immediately in the dark. To accelerate drying, it is safer to make it in a drying chamber of

thermostatically controlled oven. Note that drying at a temperature superior than 70ºC is liable to damage the board.

Step 4: Positive original

The original drawing of the circuit of printed in an acetate sheet. By doing so, the drawing will be the positive and will be copied to the board surface. The sheet is placed on top of the board surface and into the exposure chamber, where is creates vacuum to avoid light leaks underneath the drawing.

Step 5: Exposure

The varnish Positiv 20 is sensitive to ultraviolet rays, so an ultraviolet exposure chamber is used. The exposure time depends on the thickness of the coating, which were took approximately 2 minutes. The ultraviolet exposure chamber must be switched on earlier so that the lights can get to the full intensity.

Step 6: Developing

The plate is removed from the ultraviolet exposure chamber and is placed in a plastic tray together with the developer and agitated. This developer is a concentration of 7 grams of caustic soda (NaOH) to one litre of cold water. After approximately 2 minutes, the image of the conductor should be fully developed. If not, the board is under exposed. The circuits are now outlined in a different colour (copper) compared to the rest of the board (substrate). After developing rinse the board in running cold water to clean it and avoid over developing the board.

Step 7: Etching

Varnish Positiv 20 is resistant to acid baths of ferric chloride ($FeCl_3$). As so, the plate is etched in a bath of ferric chloride heated to approximately 45ºC of a density of 35-40%. This mixture produces pungent smells and light vapours, it has to be used in great care.

Step 8: Cleaning (removal of the coating)

For removing the coating, acetone is used. The plate is cleaned once again and is ready to be used.

The final results of the uniform and the Chebyshev arrays, already with the coaxial connection, are presented below in Fig. 4.1 and 4.2 respectively.

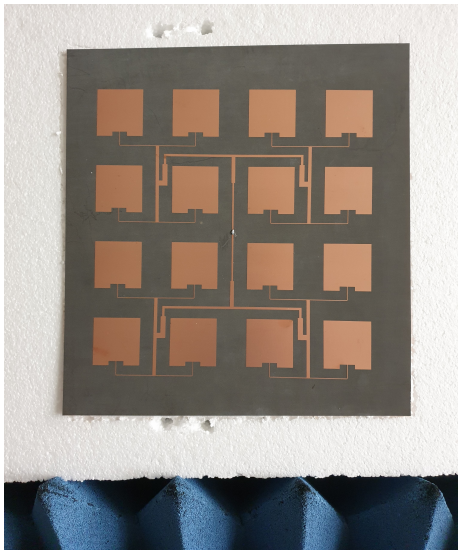

FIGURE 4.1: Constructed uniform array

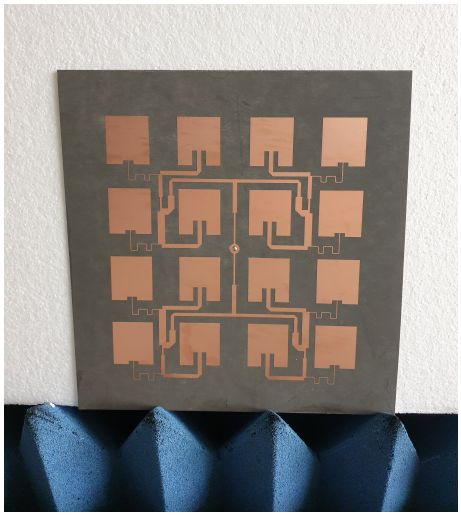

FIGURE 4.2: Constructed Chebyshev array

4.2 Measurements

4.2.1 Uniform Planar Array

The results of the magnitude of the $|S_{11}|$ are compared to the simulated $|S_{11}|$ in CST and are presented in Fig. 4.3. As one observes, the lowest point of the magnitude has increased by approximately 11 dB and is slightly dislocated to a higher frequency.

Despite the loss of power, the lowest magnitude is still at -15 dB, which is an acceptable result.

The frequency where the amplitude of $|S_{11}|$ is minimal is now at 2.49 GHz, a difference of 40 MHz. This difference is not very significant, which indicates that the antenna is acceptably matched.

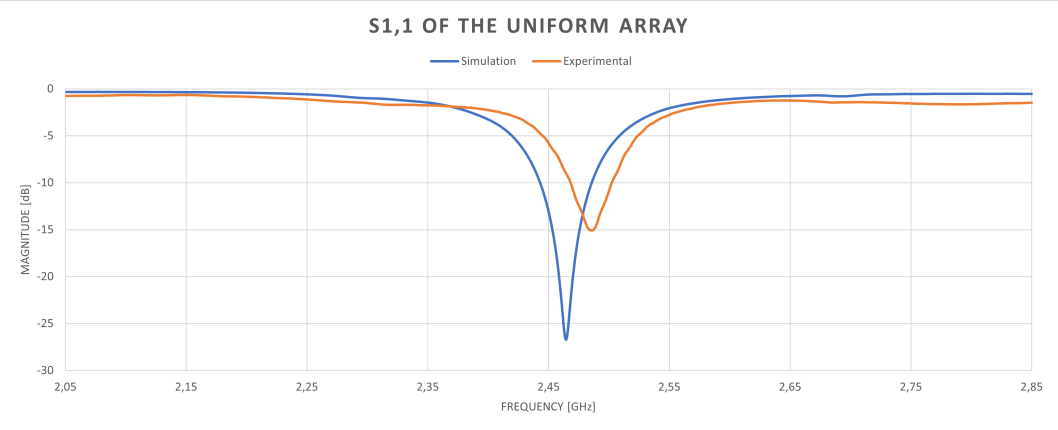

FIGURE 4.3: Comparison between the simulation and the results of the uniform array $|S_{11}|$

The experimental results of the radiation pattern in ϕ=90° show that the lowest value of the amplitude has a slight deviation in the frequency, but overall the results are similar to the simulated ones. The first null in $\theta = -30°$ is bigger than the one simulated, as the side lobes are lower.

The comparison between the simulated and the experimental results are presented in Fig. 4.4.

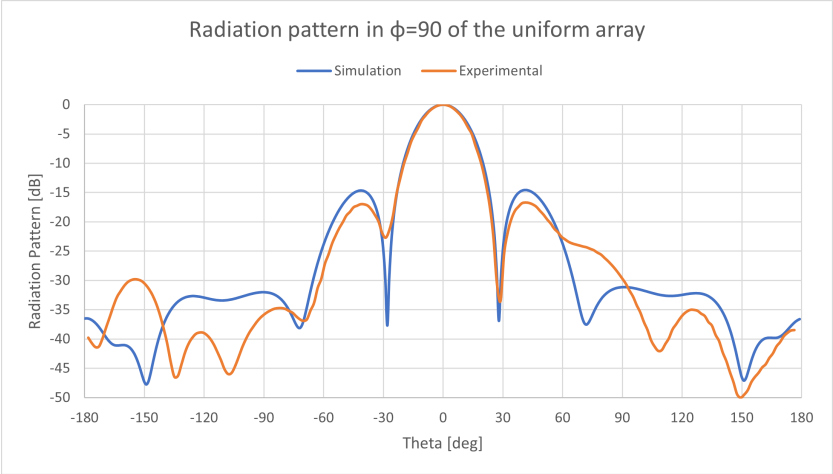

FIGURE 4.4: Comparison between the simulation and the results of the uniform array radiation pattern in ϕ=90°

As to the radiation pattern in ϕ=0°, the side lobe level has increased significantly when compared to the simulated results, as presented in Fig. 4.5.

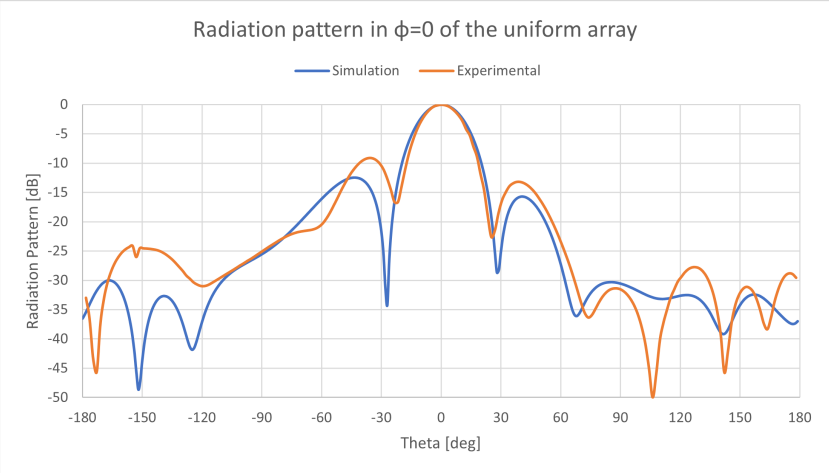

FIGURE 4.5: Comparison between the simulation and the results of the uniform array radiation pattern in ϕ=0°

4.2.2 Chebyshev Planar Array

The comparison between the simulated magnitude of the $|S_{11}|$ and the measurement results is presented in Fig. 4.6.

The lowest magnitude is at -32.2 dB, an improvement of 5.53 dB when compared to the simulated array in CST. This lowest magnitude has also jumped to an higher frequency and is now at 2.453 GHz, a difference of just 9 MHz.

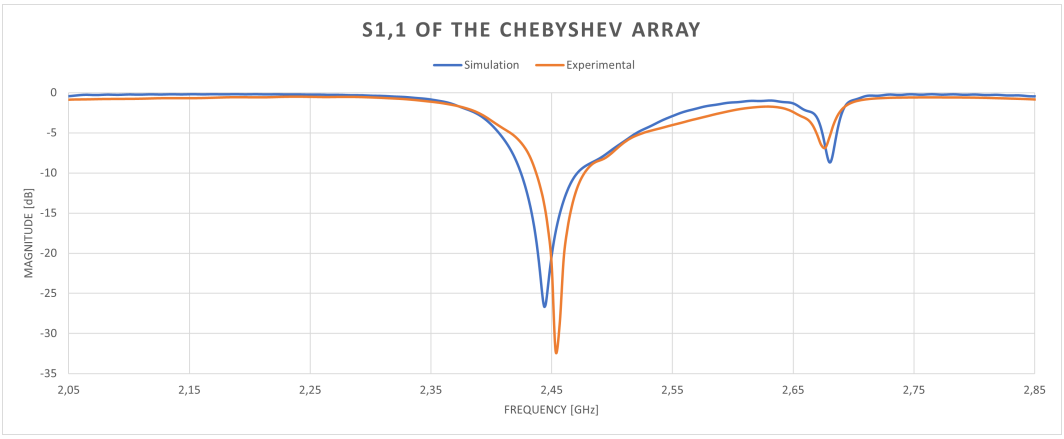

FIGURE 4.6: Comparison between the simulation and the results of the Chebyshev array $|S_{11}|$

The measured radiation pattern of the Chebyshev array in ϕ=0° shows that the lowest value of the amplitude has a slight deviation in frequency, but the overall results are as expected. The side lobes are approximately equal to the simulated results, as the null in θ=-30° is higher. The null in θ=30° is much lower that the

simulated result. However, this results show that the Chebyshev ratio is not being complied.

The comparison between the simulated and the experimental results are presented in Fig. 4.7.

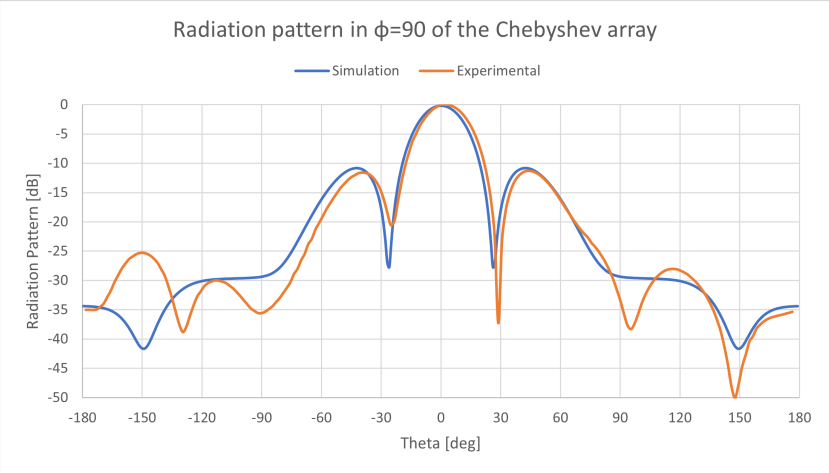

FIGURE 4.7: Comparison between the simulation and the results of the Chebyshev array radiation pattern in ϕ=90°

As to the radiation pattern in ϕ=0°, the experimental results are very different from the simulated ones. The nulls are much higher than expected and the Chebyshev ratio is not complied. The side lobe level is also much higher than expected, as presented in Fig. 4.8.

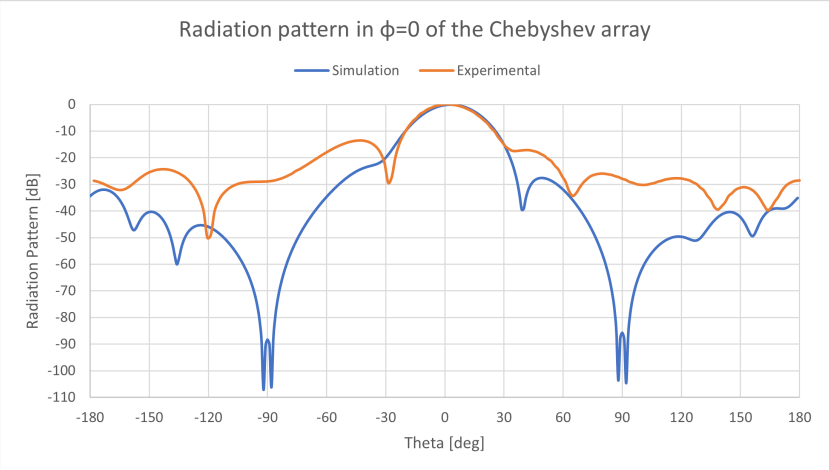

FIGURE 4.8: Comparison between the simulation and the results of the Chebyshev array radiation pattern in ϕ=0°

4.2.3 Uniform Array vs Chebyshev Array

As mentioned in Subsection 1.2.2, the main goal of a Chebyshev array is to get a low side lobe level with the narrowest beam. To understand the effects of this design method, a comparison is made between the uniform array and the Chebyshev array.

Simulated results

The simulated results of both arrays obtained in Section 3.2 are described and compared below in Tab. 4.1.

	Uniform Array	Chebyshev Array
Directivity [dB]	17.89	17.30
Total Efficiency [%]	89.6	93.3
$\|S_{11}\|$ Magnitude [dB]	-26.72	-26.67
Side Lobe Level in ϕ=0° [dB]	-12.5	-27.6
Side Lobe Level in ϕ=90° [dB]	-14.6	-10.6

Table 4.1: Comparison between the uniform array and the Chebyshev array simulations

Facing these results, one concludes that the directivity, the efficiency and the $|S_{11}|$ magnitude are similar in both arrays.

The side lobe level in ϕ=0° has decreased in the Chebyshev array and its value is close to the projected -30 dB. However, the side lobe level in ϕ=90° has increased from -14.6 dB in the uniform array to -10.6 dB in the Chebyshev array. This result is not expected accordingly to the Chebyshev design method.

Measurement results

The measurement results, presented in Section 4.2, are described and compared in Tab. 4.2 below.

	Uniform Array	Chebyshev Array
$\|S_{11}\|$ Magnitude [dB]	-15.04	-32.20
Side Lobe Level in ϕ=0° [dB]	-9.1	-13.53
Side Lobe Level in ϕ=90° [dB]	-16.7	-11.31

Table 4.2: Comparison between the uniform array and the Chebyshev array measurements

The magnitude of the $|S_{11}|$ is 17.16 dB lower in the Chebyshev array, so at an impedance level the results are positive.

This data also shows that there is an improvement in the side lobe level in ϕ=0° when the Chebyshev array is compared to the uniform array, which is a positive result. However, the value of the side lobe level in the Chebyshev array does not correspond to the calculated result nor the simulated one.

In ϕ=90°, the side lobe level of the Chebyshev array has significantly deteriorated when compared to the uniform array. This result shows that the calculated Chebyshev ratio is not being complied and the measurements do not correspond to the simulated results.

Chapter 5

Conclusion

5.1 Final Remarks

In this dissertation the theory of antenna arrays was explored in order to design arrays of patch antennas. Two arrays of patch antennas were designed with two different methods, the uniform and the Chebyshev.

The elements of the two antennas are the same and have the same spacing between them, but in the Chebyshev array the excitation coefficients are different which forces the designer to make a very different feeding network.

Although there were some limitations on the design of the patches due to the physical dimensions of the plate, the uniform array had the expected results.

On the other hand, the results of the Chebyshev array were not as expected, since the fabricated circuit measurements did not complied with the theorized values.

It is important to mention that the line widths were calculated using the expressions valid for $W/h > 1$. However, some of these widths are not valid in case and have to be recalculated for $W/h < 1$. The dispersive model was not used in this project.

At the end, one concludes that even if the results are not as expected, the use of patch antennas give the user an easy and cheap way to fabricate antennas for many applications.

5.2 Discussion

The overall project has been succeeded when it comes to the uniform array. It is expected that the experimental measurements do not correspond exactly to the

simulation due to the physical environment, but the results showed a small difference between both worlds.

The process of fabrication was careful as every step of it was fulfilled. At the end, there was even an examination of the patch in favor to correct small imperfection that the board could have.

There were some limitations when it comes to the fabrication of the antennas. On one hand, the patch did not have the dimensions needed to design both the arrays since it was too small, so that the parameter W had to be shorten in order to fabricate the antennas which required more steps in the optimization. On the other hand, there was a problem with the equipment that measures the radiation pattern, which led to a certain level of inaccuracy when the Chebyshev array was measured.

Now taking the Chebyshev array, the results were not the expected ones. The design method results were not verified in the simulation and in the experimental measurements. For a side lobe level of -30 dB, the ratio between the impedances should be 2.33, which was not enough as verified by the results. Making an analysis of the simulation, more specifically the magnitude of the elements, the results suggest that this ratio should be at least doubled in order to get the desired goal. There was also a big deterioration of the side lobe level in Phi=0^{o} when the simulation is compared to the experimental results. A lost of around 14 dB was verified in the experimental results, which suggests that something went wrong with the measurement or even the fabrication of the prototype.

5.3 Usefulness to the NAVY

This kind of technology can be easily applied in the military world since the patches are compact and cheap. They can also be easily inserted into ground stations or drones to detect targets through passive methods. This feature allows the armed forces to track and monitor their territory or even gain intelligence in certain war zone scenarios.

The low frequency used also has the benefit to visualize concealed targets that once were undetectable (Kuschel et al., 2019).

5.4 Future Work

In the future, the first steps to consider are the review of the Chebyshev array design to get the desired side lobe level. A low side lobe level will decrease the probability of the passive radar system being detected which, for the applications mentioned before, is a big advantage.

It is necessary to review the calculation of the width of the lines where $W/h < 1$, since this width mandates the characteristic impedance of the lines. The dispersive model has also to be considered in order to make a more reliable simulation.

A signal processing system is required to construct a fully functional passive radar, so it is important to make advancements in this area. A passive SAR radar requires a high computational power due to the complex signal processing. All together, the robust system can be implemented in all kinds of applications.

References

EZForm. (2022). *EZ-86-AL*. https://www.ezform.com/product/ez-86-al-2/

Gromek, D., Kulpa, K., & Samczynski, P. (2016). Experimental results of passive sar imaging using dvb-t illuminators of opportunity (C. A. Balanis, Ed.). *IEEE Geoscience and Remote Sensing Letters*, *13*, 1124–1128. https://doi.org/10.1109/LGRS.2016.2571901

Islam, S., Ibrahimy, M. I., Motakabber, S. M. A., & Hossain, A. K. M. Z. (2018). A Rectangular Inset-Fed Patch Antenna with Defected Ground Structure for ISM Band. *2018 7th International Conference on Computer and Communication Engineering (ICCCE)*, 104–108.

Kuschel, H., & O'Hagan, D. (2010). Passive radar from history to future. *4th Microwave and Radar Week MRW-2010 - 11th International Radar Symposium, IRS 2010 - Conference Proceedings*, 202–205.

Kuschel, H., Cristallini, D., & Olsen, K. E. (2019). Tutorial: Passive radar tutorial. *IEEE Aerospace and Electronic Systems Magazine*, *34*(2), 2–19. https://doi.org/10.1109/MAES.2018.160146

Orfanidis, S. J. (2004). *Electromagnetic Waves and Antennas* (Vol. 2). https://doi.org/10.1016/B978-075064947-6/50011-3

Simulia, D. S. (2022). *CST STUDIO SUITE*. https://www.3ds.com/products-services/simulia/products/cst-studio-suite/

Tsoulos, G. V., & Christodoulou, C. G. (2007). Arrays and Smart Antennas (C. A. Balanis, Ed.). *Modern Antenna Handbook*, 529–580. https://doi.org/10.1002/9780470294154.ch11

Appendix A - MATLAB Routine To Design a Patch Antenna

```
%-------------------
%NUMERIC FORMULATION TO THE SIZING OF A PATCH ANTENNA ARRAY
%Author: ASPOF EN-AEL Miguel Dias Ribeiro
%-------------------

%OBJECTIVES: Calculate the sizing of the patch antenna and its inset.

%-------------------
%CONSTANTS
%-------------------
c=3*(10^8);

%-------------------
%INPUT VALUES
%-------------------
f= input('Input the frequency (GHz): ');
f0= f*(10^9);
Er= input('Input the Er value: ');
h_mm= input('Input the hsub(mm) value: ');
h_m= h_mm/1000;
Z0= input('Input the impedance value (ohm): ');

labda0= c/f0;
k0= (2*pi)/labda0;

%-------------------
%OBTAINED RESULTS
%-------------------
W_m= (c/(2*f0))*sqrt(2/(Er+1));
W_mm= W_m*1000;
Eeff= ((Er+1)/2)+((Er-1)/2)*(1+12*(h_m/W_m))^(-1/2);
labdag= (1/sqrt(Eeff))*(c/f0);
deltaL= 0.412*h_m*((Eeff+0.3)*((W_m/h_m)+0.264))/((Eeff-0.258)*((W_m/
    h_m)+0.8));
Leff= labdag/2;
L= Leff-(2*deltaL);
L_mm= L*1000;
G= (W_m/(120*labda0))*(1-(((k0*h_m)^2)/(24)));
Za= 1/(2*G);
Wi= labda0/50;
Wi_mm= Wi*1000;
```

```
41 Li= (L/pi)*acos(sqrt(Z0/Za));
42 Li_mm= Li*1000;
43
44 %----------------------
45 %RESULTS DISPLAY
46 %----------------------
47 fprintf('The value of W is: %f mm.\n', W_mm);
48 fprintf('The value of L is: %f mm.\n', L_mm);
49 fprintf('The value of Wi is: %f mm.\n', Wi_mm);
50 fprintf('The value of Li is: %f mm.\n', Li_mm);
51
52 %----------------------
53 %END
54 %----------------------
```

SOURCE CODE A.1: MATLAB routine for patch sizing